

# CHEMISTRY

## A European Journal

A Journal of



### Accepted Article

**Title:** Photoinduced Electron Transfer in 9-Substituted 10-Methylacridinium Ions

**Authors:** Takeshi Tsudaka, Hiroaki Kotani, Kei Ohkubo, Tatsuo Nakagawa, Nikolai V. Tkachenko, Helge Lemmetyinen, and Shunichi Fukuzumi

This manuscript has been accepted after peer review and appears as an Accepted Article online prior to editing, proofing, and formal publication of the final Version of Record (VoR). This work is currently citable by using the Digital Object Identifier (DOI) given below. The VoR will be published online in Early View as soon as possible and may be different to this Accepted Article as a result of editing. Readers should obtain the VoR from the journal website shown below when it is published to ensure accuracy of information. The authors are responsible for the content of this Accepted Article.

**To be cited as:** *Chem. Eur. J.* 10.1002/chem.201604527

**Link to VoR:** <http://dx.doi.org/10.1002/chem.201604527>

Supported by  
**ACES**

WILEY-VCH

## Organophotocatalyst

# Photoinduced Electron Transfer in 9-Substituted 10-Methylacridinium Ions

Takeshi Tsudaka,<sup>[a]</sup> Hiroaki Kotani,<sup>[b]</sup> Kei Ohkubo,<sup>\*,[a,c,d]</sup> Tatsuo Nakagawa,<sup>[e]</sup> Nikolai V. Tkachenko,<sup>\*,[f]</sup> Helge Lemmetyinen,<sup>\*,[f]</sup> and Shunichi Fukuzumi<sup>\*,[c,g]</sup>

**Abstract:** A series of 9-substituted 10-methylacridinium ions (Acr<sup>+</sup>-R), in which an electron donor moiety (R) is directly linked with an electron acceptor moiety (Acr<sup>+</sup>) at the 9-position, has been synthesized and the photodynamics has been fully investigated to determine the rate constants of both the photoinduced electron transfer and back electron transfer. The driving forces of photoinduced electron transfer and back electron transfer have been determined by the electrochemical and photophysical measurements. The driving force dependence of the electron-transfer (ET) rate constants has been well analyzed in light of the Marcus theory of electron transfer. The quantum yields of formation

of the triplet ET states vary significantly depending on the interaction between the donor (R) and acceptor (Acr<sup>+</sup>) moieties. Among Acr<sup>+</sup>-R examined, 9-mesityl-10-methylacridinium ion (Acr<sup>+</sup>-Mes) exhibits the best performance in terms of the lifetime of the triplet ET state and the quantum yield. The photoexcitation of 9-mesityl-10-methylacridinium ion (Acr<sup>+</sup>-Mes) results in formation of the triplet ET state [<sup>3</sup>(Acr<sup>+</sup>-Mes<sup>+</sup>)], which has a long lifetime, a high energy (2.37 eV) and a high quantum yield (>75%) in acetonitrile. The triplet ET state delivers both the oxidizing and reducing activity of the Mes<sup>+</sup> and Acr<sup>+</sup> moieties, respectively.

## Introduction

The natural photosynthetic reaction center utilizes sequential multi-step electron transfer from the excited chromophore to the

terminal electron acceptor via electron mediators, which are well organized in a protein matrix, to attain a long lifetime of the fine charge-separated (CS) state as long as 1 second.<sup>[1-3]</sup> Extensive efforts have been devoted to develop artificial systems mimicking the photosynthetic reaction center.<sup>[4-11]</sup> The best molecular mimicking multi-step electron transfer processes in the photosynthetic reaction center so far reported is a ferrocene *meso,meso*-linked porphyrin trimer-fullerene pentad (Fc-(ZnP)<sub>3</sub>-C<sub>60</sub>) where the C<sub>60</sub> and the ferrocene (Fc) are tethered at both the ends of (ZnP)<sub>3</sub> (R<sub>ee</sub> = 46.9 Å).<sup>[12]</sup> The lifetime of the final CS state (0.53 s at 163 K) has been attained without lowering the CS efficiency (Φ = 0.83).<sup>[12]</sup> However, a significant amount of energy is lost during the multi-step electron transfer processes to reach the final CS state (0.50 eV).<sup>[1]</sup> In the photosynthesis, two-step photoexcitation, so called “Z-scheme” is thereby required to recover the energy loss via the multi-step electron transfer processes and to gain the high oxidizing power to oxidize water as well as the high reducing power to reduce NAD coenzyme.<sup>[1,13]</sup>

It is highly desired to design simple molecular dyads which are capable of fast charge separation but retain slow charge recombination.<sup>[14]</sup> Theoretically it is possible to obtain such an electron donor-acceptor dyad based on the classic Marcus theory of electron transfer [Equation (1)].<sup>[15]</sup> Herein *V* is the electronic

$$k_{\text{ET}} = \left( \frac{4\pi^3}{h^2 \lambda k_B T} \right)^{1/2} V^2 \exp \left[ -\frac{(\Delta G_{\text{ET}} + \lambda)^2}{4\lambda k_B T} \right] \quad (1)$$

coupling matrix element, *h* is the Planck constant, and *T* is the absolute temperature. According to Equation (1), logarithm of the ET rate constant (log *k*<sub>ET</sub>) is related parabolically to the ET driving force (negative ET free energy change) between electron donors

- [a] Prof. Dr. K. Ohkubo, T. Tsudaka  
Department of Material and Life Science  
Graduate School of Engineering, Osaka University and  
SENTAN, Japan Science and Technology Agency (JST)  
Suita, Osaka 565-0871 (Japan)
- [b] Prof. Dr. H. Kotani  
Department of Chemistry, Graduate School of Pure and Applied  
Sciences, University of Tsukuba, 1-1-1 Tennoudai, Tsukuba, Ibaraki  
305-8571 (Japan)
- [c] Prof. Dr. K. Ohkubo, Prof. Dr. S. Fukuzumi  
Department of Chemistry and Nano Science,  
Ewha Womans University, Seoul 120-750 (Korea)  
E-mail: fukuzumi@chem.eng.osaka-u.ac.jp
- [d] Prof. Dr. K. Ohkubo,  
Division of Applied Chemistry, Graduate School of Engineering,  
Osaka University, Suita, Osaka 565-0871 (Japan)  
Tel: (+81) 6-6879-4131  
E-mail: ookubo@chem.eng.osaka-u.ac.jp
- [e] Dr. T. Nakagawa,  
Unisoku Co., Ltd, SENTAN, Japan Science and Technology Agency  
(JST), Hirakata, Osaka 573-0131 (Japan)
- [f] Prof. Dr. N. V. Tkachenko, Prof. Dr. H. Lemmetyinen  
Institute of Materials Chemistry, Tampere University of Technology,  
P.O. Box 541, FIN-33101 Tampere, Finland, E-mail:  
nikolai.tkachenko@tut.fi, helge.lemmetyinen@tut.fi
- [g] Prof. S. Dr. Fukuzumi  
Faculty of Science and Technology, Meijo University  
SENTAN, Japan Science and Technology Agency (JST)  
Nagoya, Aichi 468-8502 (Japan)

Supporting information for this article is available on the WWW  
under <http://www.chemeurj.org/> or from the author.

and acceptors ( $-\Delta G_{ET}$ ), and the ET reorganization energy ( $\lambda$ ), that is, the energy required to structurally reorganize the donor, acceptor and their solvation spheres upon ET. It is now well recognized that the parabolic driving force dependence of  $\log k_{ET}$  provides the theoretical basis for understanding ET processes in photosynthesis the  $\log k_{ET}$  value increases with increasing the ET driving force ( $-\Delta G_{ET}$ ). When the magnitude of the driving force becomes the same as the reorganization energy ( $-\Delta G_{ET} = \lambda$ ), the reaction rate reaches a maximum and is basically controlled by the magnitude of electronic coupling ( $V$ ) between the donor and acceptor moiety [Equation (1)]. Upon passing this thermodynamic maximum, the highly exothermic region of the parabola ( $-\Delta G_{ET} > \lambda$ ) is entered, in which an additional increase of the driving force results in an actual slow-down of the reaction rate, due to an increasingly poor vibrational overlap of the product and reactant wave functions. This highly exergonic range is generally referred to as the Marcus inverted region.<sup>[15]</sup> In such a case, the magnitude of the reorganization energy is the key parameter to control the ET process. The smaller the reorganization energy, the faster is the forward photoinduced CS process, but the CR process becomes slower when the driving force for back electron transfer ( $-\Delta G_{ET}$ ) is larger than the ET reorganization energy ( $\lambda$ ). Thus, the CS lifetimes can be finely controlled by the  $\lambda$  value, which is determined by the choice of the donor and acceptor pair, the type of linkage between the donor and acceptor molecules and also the solvent.

We reported the design and synthesis of a simple electron donor-acceptor linked molecule with a small  $\lambda$  value and a high-lying triplet excited state. Acridinium ion is the best candidate for such a purpose, since the  $\lambda$  value for the electron self-exchange between the acridinium ion and the corresponding one-electron reduced radical is the smallest (0.3 eV) among the redox active organic compounds.<sup>[16]</sup> An electron donor moiety (mesityl group) is directly connected at the 9-position of the acridinium ion to yield 9-mesityl-10-methylacridinium ion ( $Acr^+-Mes$ ),<sup>[17]</sup> in which the solvent reorganization of ET is minimized because of the short linkage between the donor and acceptor moieties.<sup>[16]</sup> The photoexcitation of  $Acr^+-Mes$  affords the long-lived electron-transfer (ET) state with a virtually infinite lifetime of the electron-transfer state ( $Acr^+-Mes^{*+}$ ) at 77 K, a high energy (2.37 eV) and a high quantum yield close to unity (98%).<sup>[17]</sup> Because the charge is not separated in electron transfer from the Mes moiety to the singlet excited state of the  $Acr^+$  moiety, we denote the resulting state as the ET state. The long-lived ET state was questioned by Benniston et al. who reported that the triplet energy (1.96 eV) of the  $Acr^+$  moiety of  $Acr^+-Mes$  was lower than the ET state.<sup>[18]</sup> Such a triplet excited state of the  $Acr^+$  moiety of  $Acr^+-Mes$  would never be able to oxidize electron donors which have the one-electron oxidation potentials higher than the one-electron reduction potential of the triplet excited state of the  $Acr^+$  moiety of  $Acr^+-Mes$  ( $E_{red}^+$  vs. SCE = 1.53 V).<sup>[19]</sup> By the same token, the triplet excited state of the  $Acr^+$  moiety of  $Acr^+-Mes$  would never be able to reduce electron acceptors which have the one-electron reduction potentials lower than the one-electron oxidation potential of the triplet locally excited state of  $Acr^+-Mes$  ( $E_{ox}^+$  vs. SCE = 0.07 V), either.<sup>[19]</sup> However, the photoexcitation of  $Acr^+-Mes$  with electron donors and/or acceptors resulted in electron-transfer oxidation of a variety of electron donors which have much higher one-electron oxidation potentials than 1.53 V,<sup>[20-22]</sup> and also electron-transfer reduction of hexyl viologen which has the much lower one-

electron reduction potential ( $E_{red}$  vs. SCE = -0.43 V) than 0.07 V.<sup>[23]</sup> Thus, a variety of photoredox catalytic reactions including oxygenation, cycloadditions, atom transfer cyclizations, C-H functionalizations, alkene hydrofunctionalizations and bond cleavage reactions have been made possible by utilizing the high oxidizing and reducing ability of the  $Mes^{*+}$  and  $Acr^+$  moiety of the ET state, respectively.<sup>[20-27]</sup> The triplet locally excited state of  $Acr^+-Mes$  would never be able to be utilized for variety of photoredox catalytic reactions due to the lack of the oxidizing or reducing ability. However, the systematic photodynamic- including the intersystem crossing from the singlet ET state to the triplet ET state of  $Acr^+-Mes$  and other derivatives have yet to be examined. The oxidizing and reducing ability of the photogenerated species of  $Acr^+-Mes$  (singlet and triplet ET locally excited triplet) has yet to be fully clarified, either.

We report herein the synthesis and photodynamics of a series of 9-substituted 10-methylacridinium ions ( $Acr^+-R$ , R = donor moieties such as alkylbenzene, naphthalene, and anthracene derivatives), in which R is directly linked with an electron acceptor moiety ( $Acr^+$ ) at the 9-position. The redox and photophysical properties were scrutinized including the intersystem crossing to analyze the driving force dependence of the rate constants of photoinduced electron transfer and back electron transfer in light of the Marcus theory of electron transfer. In order to examine the nanosecond time range in a wide spectral range, we have applied a newly developed randomly-interleaved-pulse-train (RIPT) method in this study.<sup>[28]</sup> The surprisingly long lifetime of the triplet ET state of  $Acr^+-Mes$ , which exhibited the best performance among  $Acr^+-R$  is well rationalized based on the driving force dependence of the rate constants of electron transfer and also by the subtle difference in the interaction between the donor and acceptor moieties. The oxidizing and reducing ability of the triplet ET state of  $Acr^+-Mes$  is well analyzed in light of the Marcus theory of electron transfer.

## Experimental Section

**Materials:** Benzonitrile (PhCN) used as a solvent were distilled by  $P_2O_5$  *in vacuo*.<sup>[29]</sup> Acetonitrile (MeCN) and chloroform ( $CHCl_3$ ) were used as received. Naphthalene and 1-bromonaphthalene used as electron donors were obtained commercially and used as received.  $\epsilon$ -Phenylacridine, 10-methylacridinium ion ( $AcrH^+$ ) and 7,7,8,8-tetracyanoquinodimethane (TCNQ) were purchased from Tokyo Chemical Industry Co., Ltd. Deuterated [ $^2H_3$ ]acetonitrile ( $CD_3CN$ ) was obtained from EURI SO-TOP, CEA, France and used as received.  $\zeta$ -Benzoquinone supplied by Aldrich, was purified by vacuum sublimation. 1-Benzyl-1,4-dihydropyridinamide (BNAH),<sup>[30]</sup> 1-benzyl-1,4-dihydropyridinamide dimer [ $(BNA)_2$ ]<sup>[31]</sup> and 1,1-dihexyl-4,4-dipyridinium diperchlorate [ $HV^{2+}(ClO_4^-)_2$ ]<sup>[32,33]</sup> were prepared according to the literature.

**Syntheses of  $Acr^+-R$ :** 9-Substituted 10-methylacridinium perchlorates ( $Acr^+-R ClO_4^-$ ) were prepared by the reaction of 10-methylacridone in dichloromethane with the corresponding Grignard reagents (RMgBr), then addition of sodium hydroxide for the hydrolysis and perchloric acid for the neutralization, and purified by recrystallization from ethanol-diethyl ether. 9-(1-Naphthyl)-10-methylacridinium ( $Acr^+-1NA$ ) perchlorate:  $^1H$  NMR ( $CD_3CN$ , 300 MHz)  $\delta$  (ppm) 8.64 (d,  $J = 9.0$  Hz, 2H), 8.28-8.38 (m, 3H), 8.15 (d,  $J = 9.0$  Hz, 1H), 7.72-7.80 (m, 5H), 7.60 (d,  $J = 9.0$  Hz, 2H), 7.32 (t,  $J =$

9.0 Hz, 1H), 6.94 (d,  $J = 9.0$  Hz, 1H), 4.88 (s, 3H). Anal. Calcd for  $C_{24}H_{18}ClNO_4 \cdot 0.5(H_2O)$ : C, 67.21; H, 4.47; N, 3.27. Found: C, 67.51; H, 4.32; N, 3.30. 9-(2-Naphthyl)-10-methylacridinium ( $Acr^+-2NA$ ) perchlorate:  $^1H$  NMR ( $CD_3CN$ , 300 MHz)  $\delta$  (ppm) 8.62 (d,  $J = 9.0$  Hz, 2H), 8.35-8.41 (m, 2H), 8.24 (d,  $J = 9.0$  Hz, 1H), 8.03-8.13 (m, 5H), 7.71-7.84 (m, 4H), 7.60 (d,  $J = 9.0$  Hz, 1H), 4.85 (s, 3H). Anal. Calcd for  $C_{24}H_{18}ClNO_4 \cdot 0.25(H_2O)$ : C, 67.93; H, 4.39; N, 3.30. Found: C, 67.81; H, 4.32; N, 3.34. 9-[2-(6-Methoxynaphthyl)]-10-methylacridinium ( $Acr^+-2NA(6-OMe)$ ) perchlorate:  $^1H$  NMR ( $CD_3CN$ , 300 MHz)  $\delta$  (ppm) 8.63 (d,  $J = 9.0$  Hz, 2H), 8.40 (t,  $J = 9.0$  Hz, 2H), 8.14 (d,  $J = 9.0$  Hz, 3H), 7.98 (t,  $J = 9.0$  Hz, 2H), 7.85 (t,  $J = 9.0$  Hz, 2H), 7.57 (t,  $J = 9.0$  Hz, 2H), 7.36 (d,  $J = 9.0$  Hz, 1H), 4.86 (s, 3H), 4.02 (s, 3H). Anal. Calcd for  $C_{25}H_{20}ClNO_5 \cdot 0.5(H_2O)$ : C, 65.43; H, 4.61; N, 3.05. Found: C, 65.56; H, 4.46; N, 3.04. 9-[1-(2-Methylnaphthyl)]-10-methylacridinium ( $Acr^+-1NA(2-Me)$ ) perchlorate:  $^1H$  NMR ( $CD_3CN$ , 300 MHz)  $\delta$  (ppm) 8.67 (d,  $J = 9.0$  Hz, 2H), 8.37 (t,  $J = 9.0$  Hz, 2H), 8.20 (d,  $J = 9.0$  Hz, 1H), 8.07 (d,  $J = 9.0$  Hz, 1H), 7.66-7.75 (m, 5H), 7.49 (t,  $J = 9.0$  Hz, 1H), 7.22 (t,  $J = 9.0$  Hz, 1H), 6.68 (d,  $J = 9.0$  Hz, 1H), 4.89 (s, 3H), 1.96 (s, 3H). Anal. Calcd for  $C_{25}H_{20}ClNO_4 \cdot 0.2(H_2O)$ : C, 68.63; H, 4.70; N, 3.20. Found: C, 68.66; H, 4.73; N, 3.10. 9-(9-Anthryl)-10-methylacridinium ( $Acr^+-An$ ) perchlorate:  $^1H$  NMR ( $CD_3CN$ , 300 MHz)  $\delta$  (ppm) 8.99 (s, 1H), 8.70 (d,  $J = 9.0$  Hz, 2H), 8.28-8.39 (m, 4H), 7.46-7.64 (m, 6H), 7.30 (t,  $J = 9.0$  Hz, 2H), 6.97 (d,  $J = 9.0$  Hz, 2H), 4.95 (s, 3H). Anal. Calcd for  $C_{28}H_{20}ClNO_4 \cdot 0.5(H_2O)$ : C, 70.22; H, 4.42; N, 2.92. Found: C, 70.17; H, 4.34; N, 2.90. 9-(4-Tolyl)-10-methylacridinium ( $Acr^+-Tol$ ) perchlorate:  $^1H$  NMR ( $CD_3CN$ , 300 MHz)  $\delta$  (ppm) 8.59 (d,  $J = 9.0$  Hz, 2H), 8.37 (t,  $J = 9.0$  Hz, 2H), 8.05 (d,  $J = 9.0$  Hz, 2H), 7.86 (t,  $J = 9.0$  Hz, 2H), 7.57 (d,  $J = 9.0$  Hz, 2H), 7.42 (d,  $J = 9.0$  Hz, 2H), 4.81 (s, 3H), 2.56 (s, 3H). Anal. Calcd for  $C_{21}H_{18}ClNO_4$ : C, 65.71; H, 4.73; N, 3.65. Found: C, 65.55; H, 4.76; N, 3.64. 9-(2,4-Xylyl)-10-methylacridinium ( $Acr^+-Xyl$ ) perchlorate:  $^1H$  NMR ( $CD_3CN$ , 300 MHz)  $\delta$  (ppm) 8.59 (d,  $J = 9.0$  Hz, 2H), 8.34-8.40 (m, 2H), 7.81-7.91 (m, 4H), 7.33-7.41 (m, 2H), 7.16 (d, 1H), 4.82 (s, 3H), 2.50 (s, 3H), 1.83 (s, 3H). Anal. Calcd for  $C_{22}H_{20}ClNO_4$ : C, 66.42; H, 5.07; N, 3.52. Found: C, 66.17; H, 4.96; N, 3.59. 9-Mesityl-10-methylacridinium ( $Acr^+-Mes$ ) perchlorate:<sup>[17]</sup>  $^1H$  NMR ( $CD_3CN$ , 300 MHz)  $\delta$  (ppm) 8.59 (d,  $J = 9.0$  Hz, 2H), 8.37 (t,  $J = 9.0$  Hz, 2H), 7.83 (s, 4H), 7.22 (s, 2H), 4.80 (s, 3H), 2.46 (s, 3H), 1.68 (s, 6H). Anal. Calcd for  $C_{23}H_{22}ClNO_4 \cdot 0.15(H_2O)$ : C, 66.63; H, 5.42; N, 3.38. Found: C, 66.44; H, 5.22; N, 3.49. 9-Phenyl-10-methylacridinium ( $Acr^+-Ph$ ) perchlorate:  $^1H$  NMR ( $CD_3CN$ , 300 MHz)  $\delta$  (ppm) 7.5-8.6 (m, 13H), 4.83 (s, 3H). 9-Durenyl-10-methylacridinium ( $Acr^+-Dur$ ) perchlorate:  $^1H$  NMR ( $CD_3CN$ , 300 MHz)  $\delta$  (ppm) 8.61 (d,  $J = 9.0$  Hz, 2H), 8.34-8.42 (m, 2H), 7.81 (d,  $J = 9.0$  Hz, 4H), 7.34 (s, 1H), 4.81 (s, 3H), 2.33 (s, 6H), 1.57 (s, 6H). Anal. Calcd for  $C_{24}H_{24}ClNO_4 \cdot 0.3(H_2O)$ : C, 66.83; H, 5.75; N, 3.25. Found: C, 66.83; H, 5.48; N, 3.18.

**Electrochemical measurements:** Cyclic voltammetry (CV) measurements were performed at 298 K on an ALS 630B electrochemical analyzer in deaerated MeCN containing 0.1 M  $Bu_4NClO_4$  (TBAP) as supporting electrolyte. A conventional three-electrode cell was used with a platinum working electrode (surface area of 0.3 mm<sup>2</sup>) and a platinum wire as the counter electrode. The Pt working electrode (BAS) was routinely polished with a BAS polishing alumina suspension and rinsed with acetone before use. The second harmonic AC voltammetry (SHACV) measurements<sup>[35]</sup> of 9-substituted 10-methylacridinium ions were performed on a BAS 100B electrochemical analyzer. The measured potentials were recorded with respect to the  $Ag/AgNO_3$  (0.01 M) reference electrode. The redox potentials (vs.  $Ag/Ag^+$ ) are converted to those vs. SCE by adding 0.29

V.<sup>[36]</sup> All electrochemical measurements were carried out under an atmospheric pressure of argon.

#### Time-resolved absorption spectral measurements:

Femtosecond to picosecond time-resolved absorption spectra and fluorescence lifetime measurements were collected using a pump-probe technique as described elsewhere.<sup>[37]</sup> The femtosecond pulses of the Ti:sapphire generator were amplified by using a multipass amplifier (CDP-Avesta, Moscow, Russia) pumped by a second harmonic of the Nd:YAG Q-switched laser (model LF114, Solar TI' Minsk, Belorussia). The amplified pulses were used to generate second harmonic (420 nm) for sample excitation (pump beam) and a white continuum for time-resolved spectrum detection (probe beam). The samples were placed into 1 mm rotating cuvettes, and averaging of 100 pulses at 10 Hz repetition rate was used to improve signal-to-noise ratio. Typical response time of the instrument was 150 fs (fwhm). A global multi-exponential fitting procedure was applied to process the data. The procedure takes into account the instrument time response function and the group velocity dispersion of the white continuum, allowing calculation of the decay time constants and dispersion-compensated transient absorption spectra.

Time-resolved fluorescence spectra for sub-picosecond range were measured by a Photon Technology International GL-3300 with Photon Technology International GL-302, nitrogen laser/pumped dye laser system, equipped with a four channel digital delay/pulse generator (Stanford Research System Inc. DG535) and a motor drive (Photon Technology International MD-5020). Excitation wavelength was 430 nm using dimethyl-POPOP (Exciton Co., USA) as a laser dye.

Sub-nanosecond laser-induced transient absorption spectra were collected by a customized measuring system based on the recently proposed RIPT method by Nakagawa et al.<sup>[28]</sup> The pump source is passively Q-switched microchip laser, (PowerChip PNV-M0251C Teem Photonics, 1 kHz, 350 ps, 355 nm, 25  $\mu$ J), and the probe source is a supercontinuum radiation source (SC-450, Fianium, 2 MHz, 50–100 ps, 450–2000 nm). The monochromatized probe pulse with a pre-dispersive monochromator (MD200, Unisoku) which is asynchronous with a pump pulse were irradiated on the sample and the beams transmitted through the sample and its reference beam were detected by InGaAs-photodiodes (G10899-01K, 400-1600 nm Hamamatsu). A post-dispersive monochromator (CM110, Spectra Products) were positioned before the detector to minimize fluorescence signals from the sample. Si PIN photodiodes (S5972 Hamamatsu) were used to pick up the pump pulse and the probe pulses and to evaluate delay-times between them in a shot-by-shot manner. All photodiodes' outputs are recorded with a digitizing oscilloscope (HDO8038, Teledyne Lecroy) then transferred to a PC to construct the TA temporal profile. Time resolution of the system was estimated at 400 ps from the 10-90% rise time.

For nanosecond laser flash photolysis experiments, deaerated MeCN solutions of  $Acr^+-R$  were excited by an Nd:YAG laser (Continuum, SLII-10, 4-6 ns fwhm) at  $\lambda = 355$  nm with the power of 10 mJ per pulse. The transient absorption measurements in the visible and near-IR region were performed using a continuous xenon lamp (150 W) as a probe light and a photomultiplier (Hamamatsu R2949; 350–800 nm) and an InGaAs-PIN photodiode (Hamamatsu G5125-10; 800-1200 nm) as a detector, respectively. The output from the photodiodes and a photomultiplier was recorded with a digitizing oscilloscope (Tektronix, TDS3032, 300 MHz).

**Quantum yields determination.** The quantum yields of triplet ET state ( $\Phi_{\text{TE}}^{\text{T}}$ ) of  $\text{Acr}^+-\text{R}$  were determined from the comparison with the absorption band at 500 nm due to the triplet ET state observed at 1  $\mu\text{s}$  after laser excitation at 355 nm and that of  $\text{Acr}^+-\text{Mes}$  ( $\Phi_{\text{TE}}^{\text{T}} = 0.98$ ).<sup>[17]</sup> The strong fullerene triplet-triplet absorption ( $\lambda = 750$  nm,  $\epsilon = 1.8 \times 10^4$  M<sup>-1</sup> cm<sup>-1</sup> in benzene;  $\Phi_{\text{T}} = 0.98$ )<sup>[38]</sup> served as a reference to confirm the quantum yields of  $\text{Acr}^+-\text{R}$ . The minimum molar extinction coefficients of the triplet ET state of  $\text{Acr}^+-\text{R}$  at 500 nm were  $\epsilon = 3.9 \times 10^3$  M<sup>-1</sup> cm<sup>-1</sup> in MeCN and  $\epsilon = 4.1 \times 10^3$  M<sup>-1</sup> cm<sup>-1</sup> in PhCN were determined from the absorbance at 500 nm due to  $\text{Acr}^{\cdot}$  radical produced by the ET reduction of  $\text{Acr}^+-1\text{NA}$  by tetramethylsemiquinone radical anion.<sup>[16]</sup> It should be noted that the determination of the quantum yields of the triplet ET state of  $\text{Acr}^+-\text{R}$  using the  $\epsilon$  value of  $\text{Acr}^+-1\text{NA}$  affords the maximum values, because absorbance due to  $\text{R}^{\cdot}$  is somewhat overlapped with absorbance at 500 nm due to the  $\text{Acr}^{\cdot}$  moiety in the triplet ET state.

**Spectral measurements.** A standard actinometer (potassium ferrioxalate)<sup>[39]</sup> was used for the quantum yield determination of the photochemical reactions of BNAH with hexyl viologen ( $\text{HV}^{2+}$ ) in the presence  $\text{Acr}^+-\text{R}$ . Typically, a square quartz cuvette (10 mm i.d.) which contained a deaerated MeCN solution (3.0 cm<sup>3</sup>) of  $\text{Acr}^+-\text{R}$  ( $2.0 \times 10^{-4}$  M), BNAH ( $2.0 \times 10^{-4}$  M), and  $\text{HV}^{2+}$  ( $1.0 \times 10^{-3}$  M) was irradiated with monochromatized light of  $\lambda = 430$  nm from a Shimadzu RF-5300PC fluorescence spectrophotometer. Under the conditions of actinometry experiments, the actinometer and  $\text{Acr}^+-\text{R}$  absorbed essentially all of the incident light of  $\lambda = 430$  nm. The light intensity of monochromatized light of  $\lambda = 430$  nm was determined as  $2.98 \times 10^{-9}$  einstein s<sup>-1</sup>. The photochemical reaction was monitored using a Hewlett Packard 8453 diode-array spectrophotometer. The quantum yields in the absence of oxygen [ $\Phi(\text{HV}^{\cdot+})$ ] were determined from increase in absorbance of  $\text{HV}^{\cdot+}$  at 605 nm ( $\epsilon = 1.0 \times 10^4$  M<sup>-1</sup> cm<sup>-1</sup>).<sup>[40]</sup>

**ESR measurements.** The ESR spectra were taken on a JEOL X-band spectrometer (JES-RE1XE) with a quartz ESR tube (1.2 mm i.d.). The  $g$  values and the zero-field splitting parameters ( $D$  and  $E$ ) were calibrated using an  $\text{Mn}^{2+}$  marker. The  $\text{Acr}^+-\text{Mes}$  and  $\text{Acr}^+-\text{Dur}$  were generated by the electron-transfer reduction of  $\text{Acr}^+-\text{Mes}$  ( $1.0 \times 10^{-4}$  M) and  $\text{Acr}^+-\text{Dur}$  ( $1.0 \times 10^{-4}$  M) with tetramethylsemiquinone radical anion ( $1.0 \times 10^{-4}$  M) generated by comproportionation of tetramethyl-*p*-benzoquinone and tetramethyl-*p*-hydroquinone with tetra-*n*-butylammonium hydroxide. The solution containing the radical was transferred to an ESR tube under an atmospheric pressure of Ar. The hyperfine coupling constants were determined by computer simulation using a Calleo ESR Version 1.2 program coded by Calleo Scientific on a personal computer.

**Theoretical calculations.** Density-functional theory (DFT) calculations were performed on a COMPAQ DS20E computer. Geometry optimizations were carried out using the Becke3LYP functional and 6-31G(d) basis set<sup>[41]</sup> with the unrestricted Hartree-Fock (UHF) formalism and as implemented in the Gaussian 98 program.

## Results and Discussion

**Spectral and redox properties of  $\text{Acr}^+-\text{R}$ :** A series of 9-substituted 10-methylacridinium ions ( $\text{Acr}^+-\text{R}$ ) synthesized in this study are shown in Chart 1. An electron donor moiety (R) is directly linked with an electron acceptor moiety ( $\text{Acr}^+$ ) at the 9-

position to minimize the solvent reorganization of electron transfer (ET). The absorption and fluorescence spectra of  $\text{Acr}^+-\text{R}$  in acetonitrile (MeCN) are superpositions of the spectra of the component chromophores making up these molecules (see Figure S1 in Supporting information (SI)).<sup>[42]</sup> The absorption maxima and absorption coefficients due to acridinium ion moiety are virtually the same irrespective of the difference in the R moiety (see Table 1).

The chemical shifts of <sup>1</sup>H NMR spectra of the acridinium ion moiety in  $\text{Acr}^+-\text{R}$  are also the same irrespective of the difference in the R moiety (see Experimental Section). Indeed, the dihedral angle of the X-ray crystal structure of 9-mesityl-10-methylacridinium ion ( $\text{Acr}^+-\text{Mes}$ ) made by aromatic ring plane was found to be approximately perpendicular.<sup>[17]</sup> The calculated structure of  $\text{Acr}^+-\text{Mes}$  agreed with the X-ray crystal structure which exhibits that the dihedral angle is also perpendicular between the Mes and  $\text{Acr}^+$  moieties of  $\text{Acr}^+-\text{Mes}$ .<sup>[17]</sup> In such a case, the orbital interaction between the donor and acceptor moieties is minimized. In contrast, the dihedral angle of  $\text{Acr}^+-\text{P}$  is not perpendicular (68°) according to the reported crystal structure.<sup>[43,44]</sup> The dihedral angles of other 9-substituted acridinium ions were determined by DFT method with Gaussian 98 (B3LYP/6-31G(d) basis set) as listed in Table 1. The orientation between the R and  $\text{Acr}^+$  moieties is mostly orthogonal except for R = Tol, 2-NA and 2-NA(6-OMe). This indicates the introduction of a substituent at the *ortho*-position is essential to minimize the interaction between the R and  $\text{Acr}^+$  moieties (see Chart 1).

The one-electron redox potentials of  $\text{Acr}^+-\text{R}$  were determined by cyclic voltammetry measurements. The one-electron reduction process of the  $\text{Acr}^+$  moiety was observed as a well-defined reversible wave at -0.57 V for  $\text{Acr}^+-\text{Mes}$ , -0.55 V for  $\text{Acr}^+-1\text{NA}$  and -0.52 V for  $\text{Acr}^+-\text{An}$  in MeCN (see Figure S2 in SI). The one-electron reduction potentials of  $\text{Acr}^+-\text{R}$  ( $E_{\text{red}}$ ) thus determined are listed in Table 2. On the other hand, the one-electron oxidation potentials ( $E_{\text{ox}}$ ) of  $\text{Acr}^+-\text{R}$  were determined by the second harmonic AC voltammetry (SHACV) method, since the one-electron oxidation process was irreversible in the CV measurements (see Figure S3 in SI). The  $E_{\text{ox}}$  values are also listed in Table 2. The  $E_{\text{ox}}$  values agree with those of the corresponding aromatic donor compounds.<sup>[17]</sup> The one-electron

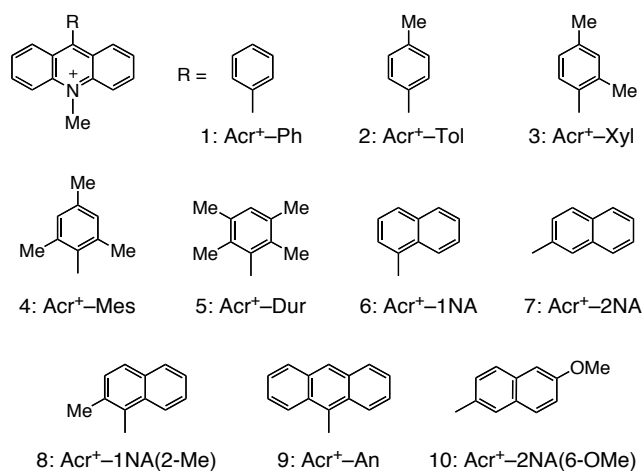


**Chart 1.** 9-Substituted acridinium ion used in this study.

**Table 1** Absorption maxima ( $\lambda_{\text{max}}$ ), absorbance coefficients ( $\epsilon$ ), fluorescence maxima ( $\lambda_{\text{fl}}$ ) and dihedral angles between acridinium ion and the donor moieties of 9-substituted 10-methylacridinium ions.

| Acr <sup>+</sup> -R          | $\lambda_{\text{max}}$ , nm | $10^{-3} \epsilon$ , $\text{M}^{-1} \text{cm}^{-1}$ [a] |          | dihedral angle [b] |  |
|------------------------------|-----------------------------|---|----------|--------------------|--|
|                              |                             | $\lambda_{\text{fl}}$ , nm                              |          | angle [b]          |  |
| Acr <sup>+</sup> -R          | 360, 425                    | 19.3, 7.50  | 501      | 62.3°              |  |
| Acr <sup>+</sup> -Tol        | 360, 423                    | 17.0, 6.50  | 500      | 88.0°              |  |
| Acr <sup>+</sup> -Xyl        | 359, 422                    | 15.8, 5.60  | 501      | 89.7°              |  |
| Acr <sup>+</sup> -Dur        | 359, 422                    | 14.3, 4.70  | 495      | 89.5°              |  |
| Acr <sup>+</sup> -1NA        | 360, 424                    | 15.5, 5.10  | 501, 590 | 89.9°              |  |
| Acr <sup>+</sup> -2NA        | 359, 428                    | 14.0, 5.90  | 500, 594 | 61.9°              |  |
| Acr <sup>+</sup> -1NA(2-Me)  | 360, 423                    | 18.2, 6.10  | 497      | 89.6°              |  |
| Acr <sup>+</sup> -An         | 359, 447                    | 15.0, 7.40  | n.d. [c] | 58.0°              |  |
| Acr <sup>+</sup> -2NA(6-OMe) | 365, 387, 422               | 21.6, 10.1, 6.50  | n.d. [c] | 89.0°              |  |

[a] In MeCN at 298 K. [b] Determined by DFT calculation (B3LYP/6-31G(d) basis set). [c] Not determined.

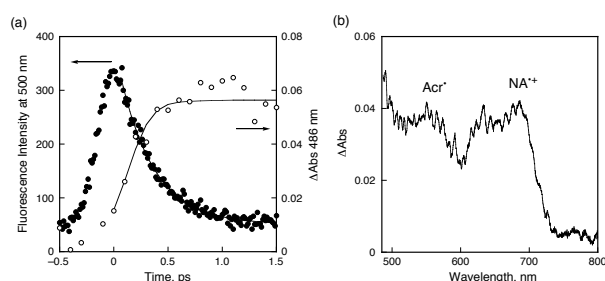


**Figure 1.** (a) Fluorescence decay time profile (●) and absorption time profile (○) of Acr<sup>+</sup>-1NA ( $1.0 \times 10^{-4}$  M) in MeCN after laser excitation at 420 nm at 298 K. (b) Transient absorption spectrum of Acr<sup>+</sup>-1NA in deaerated MeCN taken at 1.3 ps after femtosecond laser excitation at 420 nm.

redox potentials of Acr<sup>+</sup>-R were also determined in chloroform (CHCl<sub>3</sub>) and benzonitrile (PhCN) and the values are listed in Table 2.

**Formation of ET states of Acr<sup>+</sup>-R.** The fluorescence lifetimes ( $\tau$ ) of Acr<sup>+</sup>-R were measured by using femtosecond laser excitation at 420 nm (see Experimental Section). The fluorescence lifetime of the unlinked 10-methylacridinium ion

(AcrH<sup>+</sup>:  $\tau = 37$  ns in MeCN)<sup>[17]</sup> was significantly reduced when it was replaced by Acr<sup>+</sup>-1NA ( $\tau = 310$  fs) due to the quenching of the singlet excited state of Acr<sup>+</sup> by 1NA moiety (Table 2). The fluorescence decay curve of Acr<sup>+</sup>-1NA at 500 nm was well-fitted by a single-exponential decay (Figure 1a). Photoexcitation of Acr<sup>+</sup>-1NA in MeCN with femtosecond laser at 420 nm affords a transient absorption spectrum with maxima at 530 and 700 nm, which are assigned to acridinyl radical<sup>[46,47]</sup> and naphthalene radical cation,<sup>[48]</sup> respectively (Figure 1b). Thus, the transient absorption spectrum in Figure 1b can be assigned to the single<sup>+</sup> ET state [<sup>1</sup>(Acr<sup>+</sup>-1NA<sup>+</sup>)]. The rate constant of formation of the singlet ET state ( $3.4 \times 10^{12} \text{ s}^{-1}$ ) agrees with the fluorescence decay rate constant of Acr<sup>+</sup>-1NA ( $3.2 \times 10^{12} \text{ s}^{-1}$ ) in Figure 1a. Such agreement of the rate constant of formation of the single ET state with the fluorescence decay rate constant was also confirmed for Acr<sup>+</sup>-Mes in MeCN at 298 K (Figure S4 in SI).<sup>[1]</sup> The time profile of the singlet ET state of Acr<sup>+</sup>-Mes was examined by sub-nanosecond laser-induced transient absorption measurements (see Experimental Section)<sup>[28]</sup> as shown in Figure 2. The decay of the absorption band at 500 nm was accompanied by appearance of the NIR absorption around 1000 nm. The appearance of the NIR absorption was previously reported to result from the formation of the  $\pi$ -dimer radical cation between the ET state of Acr<sup>+</sup>-Mes and the ground state Acr<sup>+</sup>-Mes.<sup>[49]</sup>

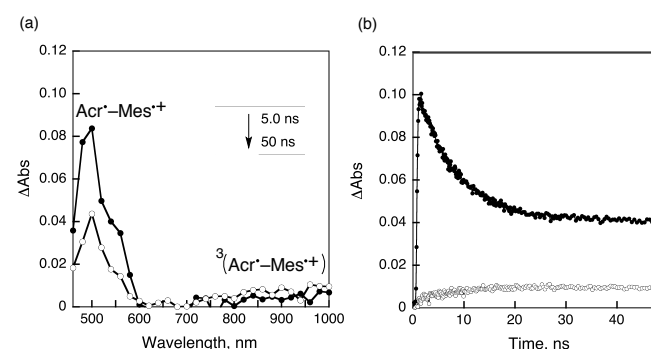


**Figure 2.** (a) Transient absorption spectra of Acr<sup>+</sup>-Mes ( $5.0 \times 10^{-4}$  M) in deaerated MeCN at 298 K taken 5 ns (●) and 50 ns (○) after laser excitation at 355 nm. (b) Time profiles of the absorbance decay at 500 nm (●) and the rise at 1000 nm (○) of Acr<sup>+</sup>-Mes ( $2.0 \times 10^{-3}$  M) in deaerated MeCN at 298 K after laser excitation at 355 nm.

**Table 2.** One-electron oxidation and reduction potentials and fluorescence lifetimes of 9-substituted 10-methylacridinium ions.

| Acr <sup>+</sup> -R          | in MeCN                    |                             | in PhCN                    |                             | in CHCl <sub>3</sub>       |                             | $\tau$ , ps         |      |                   |
|------------------------------|----------------------------|-----------------------------|----------------------------|-----------------------------|----------------------------|-----------------------------|---------------------|------|-------------------|
|                              | $E_{\text{ox}}$ vs. SCE, V | $E_{\text{red}}$ vs. SCE, V | $E_{\text{ox}}$ vs. SCE, V | $E_{\text{red}}$ vs. SCE, V | $E_{\text{ox}}$ vs. SCE, V | $E_{\text{red}}$ vs. SCE, V | MeCN                | PhCN | CHCl <sub>3</sub> |
| Acr <sup>+</sup> -Ph         | —                          | -0.55 <sup>[a]</sup>        | 2.27                       | -0.60                       | —                          | -0.47 <sup>a</sup>          | 1500 <sup>[b]</sup> | 3100 | 2200 <sup>b</sup> |
| Acr <sup>+</sup> -Tol        | —                          | -0.56                       | 2.06                       | -0.62                       | —                          | -0.46                       | 310                 | 1500 | 1200              |
| Acr <sup>+</sup> -Xyl        | 2.15                       | -0.56                       | 2.08                       | -0.61                       | 2.24                       | -0.46                       | 80                  | 200  | 120               |
| Acr <sup>+</sup> -Mes        | 2.06                       | -0.57                       | 1.88                       | -0.49                       | 2.20                       | -0.46                       | 4.2                 | 4.2  | 0.12              |
| Acr <sup>+</sup> -Dur        | 1.84                       | -0.62                       | 1.84                       | -0.62                       | 2.12                       | -0.48                       | 0.86                | 3.7  | 5.3               |
| Acr <sup>+</sup> -1NA        | 1.72                       | -0.55                       | 1.78                       | -0.57                       | 1.88                       | -0.46                       | 0.31                | 3.6  | 5.4               |
| Acr <sup>+</sup> -2NA        | 1.87                       | -0.56                       | 1.85                       | -0.60                       | 1.87                       | -0.46                       | 0.70                | 3.7  | 7.9               |
| Acr <sup>+</sup> -1NA(2-Me)  | 1.37                       | -0.54                       | 1.77                       | -0.58                       | 1.82                       | -0.44                       | 0.22                | 0.38 | 1.0               |
| Acr <sup>+</sup> -An         | 1.25                       | -0.52                       | 1.34                       | -0.57                       | 1.53                       | -0.40                       | 0.34                | 0.30 | 0.26              |
| Acr <sup>+</sup> -2NA(6-OMe) | 1.25                       | -0.57                       | 1.45                       | -0.61                       | 1.52                       | -0.48                       | 0.18                | 0.25 | 1.9               |

[a] Taken from ref. [45]. [b] Taken from ref. [46].

However, the rate of appearance of the NIR band at 1000 nm obeyed first-order-kinetics and the first-order rate constant remained constant with increasing concentration of Acr<sup>+</sup>-Mes (Figure S5 in SI). Thus, the observed spectral change in Figure 2 results from the intramolecular process, which is assigned to be intersystem crossing (ISC) from the singlet ET state to the triplet ET state. The absorption maximum remained the same at 500 nm but the absorbance decreased by ISC, whereas the NIR absorption band appeared by ISC. The similar NIR absorption band was also observed by ISC from the singlet ET state to the triplet ET state of Acr<sup>+</sup>-1NA (Figure S6 in SI). The increase in the NIR band in Figure 2 (and Figure S6 in SI) may result from the D<sub>1</sub> ← D<sub>0</sub> dipole-forbidden transition,<sup>[50-52]</sup> which becomes slightly allowed in the triplet ET state, whereas it is forbidden in the singlet ET state. Due to operation of the Pauli principle, the integrated repulsion between electrons of like spin in the triplet is lower than that between electrons of opposite spin in the singlet. Thus, the unpaired electron in the donor radical cation of the triplet ET state may be slightly more delocalized in the Acr' moiety, making the forbidden transition in the NIR region to be observable. The rate constant of the intersystem crossing of the singlet ET state of Acr<sup>+</sup>-Mes was determined from the slope of the first-order plot (Figure S5 in SI) to be 1.3 × 10<sup>8</sup> s<sup>-1</sup> at 298 K. Similarly the rate constant of the intersystem crossing of the singlet ET state of Acr<sup>+</sup>-1NA was determined to be 2.5 × 10<sup>8</sup> s<sup>-1</sup> at 298 K (Figure S6 in SI).

The transient absorption spectra of Acr<sup>+</sup>-An are shown in Figure 3a, where the absorption due to the anthracene radical

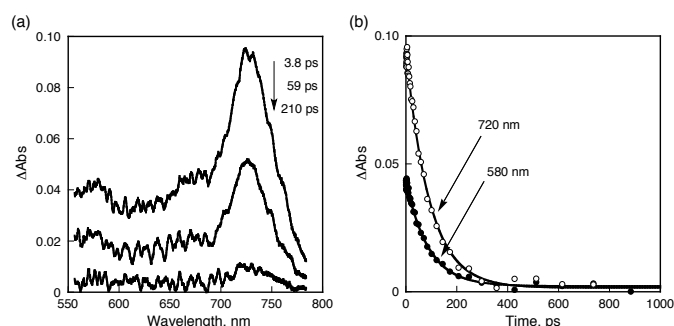


**Figure 3.** (a) Transient absorption spectra of Acr<sup>+</sup>-An (1.0 × 10<sup>-4</sup> M) in deaerated MeCN at 298 K taken after femtosecond laser excitation at 420 nm. (b) Decay time profiles of Acr<sup>+</sup>-An<sup>+</sup> at 580 and 720 nm.

cation is clearly detected at 720 nm, which agrees with the absorption maximum of anthracene radical cation.<sup>[48,53]</sup> In this case, the transient absorption at 720 nm as well as at 580 nm decays to zero in the observed time range up to 1 ns. This indicates that the singlet ET state decays to the ground state with a lifetime of 90 ps prior to the intersystem crossing to the triplet ET state. The decay to the locally excited triplet state (Acr<sup>+</sup>-<sup>3</sup>An<sup>+</sup>) is energetically unfavorable, since the triplet energy of anthracene moiety (1.84 eV)<sup>[54]</sup> is higher than that of ET state of Acr<sup>+</sup>-An (1.77 eV). The fast decay of the singlet ET state [<sup>1</sup>(Acr<sup>+</sup>-An<sup>+</sup>)] to the ground state results from the much smaller driving force as compared with the case of <sup>1</sup>(Acr<sup>+</sup>-Mes<sup>+</sup>) (vide infra).

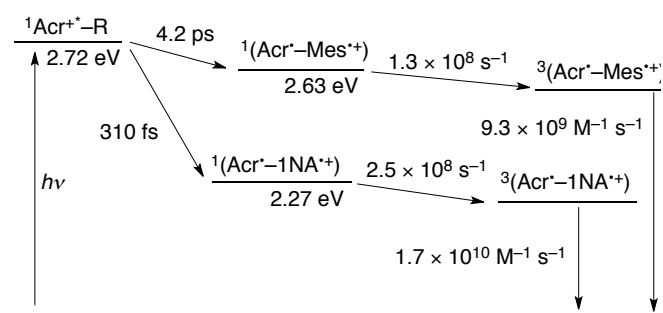
**Quantum yields of formation of the ET states of Acr<sup>+</sup>-R.** The transient absorption due to the ET state of Acr<sup>+</sup>-Mes decays in the time range up to 3 μs when the residual absorption still remains. The decay time profiles of the transient absorbance at

500 nm due to the ET states of Acr<sup>+</sup>-R are shown in Figure 4a. The decay of the ET state occurs via intermolecular back electron transfer between two <sup>3</sup>(Acr<sup>+</sup>-R<sup>+</sup>) molecules rather than intramolecular back electron transfer from the Acr' moiety to the R<sup>+</sup> moiety, because the intermolecular back electron transfer is spin-allowed, whereas the intramolecular back electron transfer is spin-forbidden. The ET state (Acr<sup>+</sup>-R<sup>+</sup>) population obeys second-order kinetics rather than first-order kinetics as indicated by the linear plot of [Acr<sup>+</sup>-R<sup>+</sup>]<sup>-1</sup> vs. time in Figure 4b, where the concentration of Acr<sup>+</sup>-R<sup>+</sup> was determined using the ε value at 500 nm of Acr<sup>+</sup>-1NA (ε = 3.9 × 10<sup>3</sup> M<sup>-1</sup> cm<sup>-1</sup> in MeCN and ε = 4.1 × 10<sup>3</sup> M<sup>-1</sup> cm<sup>-1</sup> in PhCN). In such a case, the concentration of Acr<sup>+</sup>-R<sup>+</sup> may be overestimated due to the overlap of the absorbance of the Acr' moiety at 500 nm. Thus, the second-order decay rate constants determined from the slopes of the plots in Figure 4b are regarded as the minimum values, which are already close to the diffusion-limited values as listed in Table 3. In addition, the energy diagram and photodynamics of Acr<sup>+</sup>-R (R = Mes and 1NA) in MeCN were summarized in Scheme 1.

**Table 3.** Rate constants of intermolecular back electron transfer (*k*<sub>BET</sub>) of 9-substituted 10-methylacridinium ions

| Acr <sup>+</sup> -R         | <i>k</i> <sub>BET</sub> , M <sup>-1</sup> s <sup>-1</sup> |                       |
|-----------------------------|---|-----------------------|
|                             | in MeCN   | in PhCN               |
| Acr <sup>+</sup> -Mes       | 9.3 × 10 <sup>9</sup>                                     | 3.0 × 10 <sup>9</sup> |
| Acr <sup>+</sup> -1NA       | 1.7 × 10 <sup>10</sup>                                    | 4.6 × 10 <sup>9</sup> |
| Acr <sup>+</sup> -1NA(2-Me) | [a]   | 6.9 × 10 <sup>9</sup> |
| Acr <sup>+</sup> -2NA       | [a]   | 7.9 × 10 <sup>9</sup> |

[a] Not determined.



Acr<sup>+</sup>-R (R = Mes and 1NA)

**Scheme 1.** The energy diagram and photodynamics of Acr<sup>+</sup>-R (R = Mes and 1NA)

The decay lifetime of <sup>3</sup>(Acr<sup>+</sup>-Mes<sup>+</sup>) due to intramolecular back electron transfer in MeCN at 298 K were determined to be 2.0 μs by incorporating Acr<sup>+</sup>-Mes into nanosized mesoporous silica-alumina in order to prohibit the intermolecular back electron transfer.<sup>[55]</sup> And the rate constant of <sup>3</sup>(Acr<sup>+</sup>-Mes<sup>+</sup>) due to intramolecular back electron transfer in PhCN at 298 K were also determined to be 98 s<sup>-1</sup> by the linear plot of ln(*k*<sub>BET</sub>/*T*) vs. *T*<sup>-1</sup> measured by laser flash photolysis and ESR methods.<sup>[17]</sup> The much longer lifetime of <sup>3</sup>(Acr<sup>+</sup>-Mes<sup>+</sup>) due to intramolecular back electron transfer in PhCN than that in MeCN results from the larger driving force of the back electron transfer in PhCN than that in MeCN (see the *E*<sub>ox</sub> and *E*<sub>red</sub> values in PhCN vs. MeCN in Table 2).

The initial absorbance at 500 nm is significantly different depending on the type of R in Figure 4a. The absorbance at 500 nm due to the triplet ET state of Acr<sup>+</sup>-Dur is certainly not zero in the time range up to 80 μs. This indicates that there is a long-lived component even in the case of Acr<sup>+</sup>-Dur<sup>+</sup>, which affords the smallest absorbance at 500 nm in Figure 4a.

The quantum yields of the triplet ET states ( $\Phi_{\text{TET}}$ ) of Acr<sup>+</sup>-R were determined from the initial absorbance at 500 nm due to the triplet ET state in Figure 4a (Table 4). The  $\Phi_{\text{TET}}$  values vary significantly depending on the substituted donor moieties in the series of Acr<sup>+</sup>-R. The  $\Phi_{\text{TET}}$  value of Acr<sup>+</sup>-Mes<sup>+</sup> is the largest (98%), which is close to unity. It should be noted again, however, the  $\Phi_{\text{TET}}$  value is the maximum value determined by using the  $\epsilon$  value at 500 nm of Acr<sup>+</sup>-1NA ( $\epsilon = 3.9 \times 10^3 \text{ M}^{-1} \text{ cm}^{-1}$  in MeCN and  $\epsilon = 4.1 \times 10^3 \text{ M}^{-1} \text{ cm}^{-1}$  in PhCN).

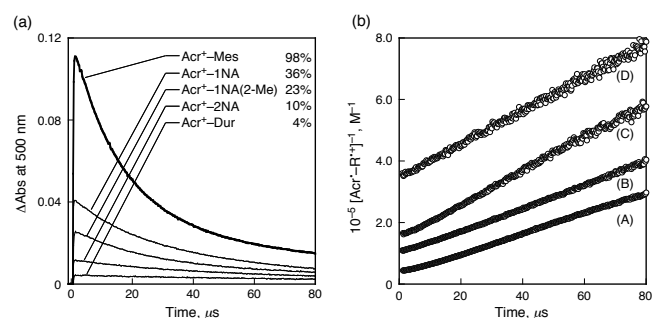


**Figure 4.** (a) Decay time profiles at 500 nm and quantum yields of formation of ET state of Acr<sup>+</sup>-R ( $5.0 \times 10^{-5} \text{ M}$ ) in PhCN at 298 K after laser excitation at 355 nm determined by the comparative method. (b) Second-order plots of the decay of the transient absorption spectra of (A) Acr<sup>+</sup>-Mes, (B) Acr<sup>+</sup>-1NA, (C) Acr<sup>+</sup>-1NA(2-Me) and (D) Acr<sup>+</sup>-2NA. MeCN at 298 K after laser excitation at 355 nm.

**Driving force dependence of intramolecular photoinduced ET and BET of Acr<sup>+</sup>-R.** The driving force of photoinduced ET ( $-\Delta G_{\text{ET}}$ ) from the 1NA to <sup>1</sup>Acr<sup>+</sup> in MeCN is determined to be 0.45 eV from the one-electron reduction potential ( $E_{\text{red}}$  vs. SCE = -0.55 V) and the excited state energy ( $^1\Delta E^* = 2.72 \text{ eV}$ ) of the Acr<sup>+</sup> moiety and the one-electron oxidation potential of the 1NA moiety ( $E_{\text{ox}}$  vs. SCE = 1.72 V) in Acr<sup>+</sup>-1NA (see Experimental Section). Similarly the  $-\Delta G_{\text{ET}}$  values of Acr<sup>+</sup>-R were determined from the  $E_{\text{ox}}$ ,  $E_{\text{red}}$  and  $^1\Delta E^*$  values. The rate constants of photoinduced ET are determined from the difference between  $\tau^{-1}$  and  $\tau_0^{-1}$ , where  $\tau$  and  $\tau_0$  are fluorescence lifetimes of Acr<sup>+</sup>-R in Table 2 and AcrH<sup>+</sup> (37 ns in MeCN, 35 ns in PhCN and 30 ns in CHCl<sub>3</sub>).<sup>[46]</sup> The driving force dependence of  $\log k_{\text{ET}}$  is shown in Figure 5. The same plot shows also rate constants obtained for BET for Acr<sup>+</sup>-2NA(6-OMe) and Acr<sup>+</sup>-An in which case the driving force was evaluated as differences between  $E_{\text{ox}}$  and  $E_{\text{red}}$ . This part of plot presents ET reactions with the same multiplicity. As mentioned above, the slowest BET was observed for Acr<sup>+</sup>-Mes, and was attributed to the triplet ET state for which electronic coupling may differ gradually from that of the singlet BET state. Also the driving force may be expected to be somewhat smaller for the triplet BET compared to that of the singlet one. All the points including the BET in Acr<sup>+</sup>-Mes form a bell-shape dependence expected for Marcus-type photoinduced ET and BET processes. If modeled by Equation (1),<sup>[15]</sup> the values  $\lambda = 0.92 \text{ eV}$  and  $V = 330 \text{ cm}^{-1}$  can be obtained. However, it is known that the classic Marcus theory describes poorly so-called inverted region ( $-\Delta G_{\text{ET}} > \lambda$ , in this case), the obtained value of electronic coupling is too large to treat vibrational motion classically, and, more importantly,  $V$  is

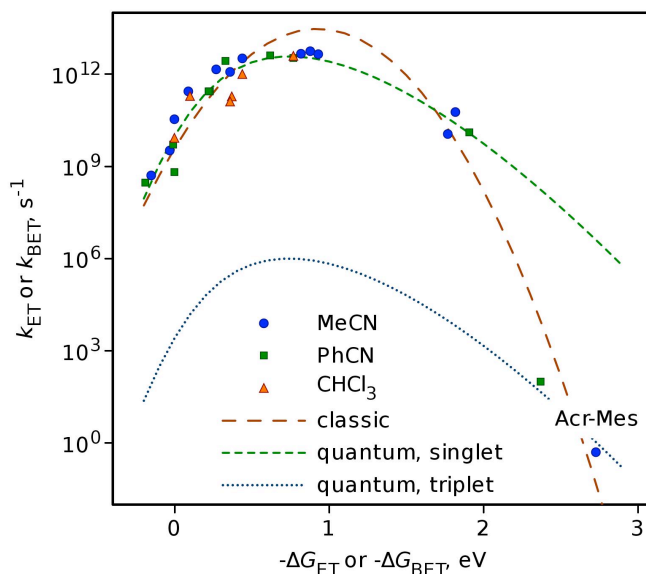


**Figure 5.** Driving force ( $-\Delta G_{\text{ET}}$  or  $-\Delta G_{\text{BET}}$ ) dependence of the logarithm of intramolecular ET and BET rate constants ( $\log k_{\text{ET}}$  or  $\log k_{\text{BET}}$ ) in Acr<sup>+</sup>-R in MeCN (●), PhCN (■) and CHCl<sub>3</sub> (▲) at 298 K.

expected to be very different for reactions involving the single and triplet ET states. A better approximation can be achieved by using semi-quantum theory or using Equation (2),

$$k_{\text{ET}}^q = \frac{2\pi^{3/2}}{h} \frac{V^2}{\sqrt{\lambda_0 k_B T}} \sum_{i=0}^{\infty} e^{-S} \frac{S^i}{i!} \exp \left[ -\frac{(\Delta G_{\text{ET}} + \lambda_0 + iE_v)^2}{4\lambda_0 k_B T} \right] \quad (2)$$

where  $E_v$  is the vibrational frequency,  $S$  is the electronic vibrational coupling, and  $\lambda_0$  is the outer sphere reorganization energy in this case. The internal reorganization energy can be calculated as  $\lambda = E_v/S$ . The fit of the data involving the singlet ET states only is shown in Figure 5 by the green dashed line, and yields  $V = 130 \text{ cm}^{-1}$ ,<sup>[56]</sup>  $\lambda_0 = 0.48 \text{ eV}$ ,  $E_v = 0.17 \text{ eV}$ , and  $S = 1.5$ . The corresponding internal reorganization energy is  $\lambda = 0.32 \text{ eV}$  and the total reorganization energy  $\lambda = \lambda_0 + \lambda = 0.8 \text{ eV}$ . The semi-quantum theory predicts somewhat lower reorganization energy, essentially lower electronic coupling, and gives much better data approximation, but the rates of the triplet ET reaction (two points in the right-bottom corner of the plot) lay completely outside this dependence. The latter is expected since the triplet ET reaction must have much lower  $V$ . Actually all other parameters describing ET dependence ( $E_v$ ,  $\lambda_0$ , and  $S$ ) are associated with nuclear subsystem and should be insensitive to the multiplicity at least to the first approximation. Assuming that only  $V$  differs the reactions involving singlet and triplet ET states, the dotted curve was generated in Figure 5. This curve predicts the electronic coupling for the triplet ET reactions to be  $V_T = 0.07 \text{ cm}^{-1}$ , or much smaller than that for the singlet ET, as expected.

Over all the  $\lambda$  value corresponds to that of the intermolecular photoinduced ET from various alkylbenzenes to <sup>1</sup>AcrH<sup>+</sup> in MeCN (0.88 eV).<sup>[16]</sup> In the normal region of the Marcus parabola ( $-\Delta G_{\text{ET}} < \lambda$ ), the  $k_{\text{ET}}$  value increases with increasing the  $-\Delta G_{\text{ET}}$  value. Thus, the  $k_{\text{ET}}$  value of Acr<sup>+</sup>-Ph ( $4.8 \times 10^8 \text{ s}^{-1}$ ) in the Marcus normal region is much smaller than the  $k_{\text{ET}}$  value of Acr<sup>+</sup>-2NA(6-OMe) ( $5.6 \times 10^{12} \text{ s}^{-1}$ ) at the top region ( $-\Delta G_{\text{ET}} \approx \lambda$ ) (see Figure S7

in SI). On the other hand, the rate constant of intramolecular back electron transfer (BET) in the case of  $^1(\text{Acr}^+-\text{An}^+)$  (Figure 3) fits well the Marcus semi-quantum curve in the inverted region. Whereas the BET rates for  $^3(\text{Acr}^+-\text{Mes}^+)$ , which were determined by using  $\text{Acr}^+-\text{Mes}$  incorporated into nanosized mesoporous silica-alumina in MeCN,<sup>[55]</sup> can be used to compare the electronic couplings for the ET reactions with the same and changing multiplicities.

It should be noted that the second-order rate constants of intermolecular back electron transfer in Table 3 cannot be plotted in Figure 5. The predominant intermolecular back electron transfer as compared with the slow intramolecular back electron transfer may result from the much larger solvent reorganization energy for the intermolecular back electron transfer as observed for solvent-separated radical ion pair.<sup>[57]</sup>

**Oxidizing and reducing ability of  $\text{Acr}^+-\text{Mes}^+$ .** We have previously reported the photocatalytic one-electron reduction of hexyl viologen ( $\text{HV}^{2+}$ ) by an NADH analogue, 1-benzyl-1,4-dihydronicotin amide (BNAH) to produce two equivalents of the one-electron reduced species ( $\text{HV}^{\cdot+}$ ) and one-equivalent of the two-electron oxidized species ( $\text{BNA}^{\cdot}$ ).<sup>[40]</sup> The quantum yields of formation of  $\text{HV}^{\cdot+}$  [ $\Phi(\text{HV}^{\cdot+})$ ] in Table 4 were determined by using  $\text{Acr}^+-\text{R}$  as a photocatalyst (see Experimental Section).<sup>[58]</sup> The largest  $\Phi(\text{HV}^{\cdot+})$  value is obtained in the case of the photoreduction of  $\text{HV}^{2+}$  by 1-benzyl-1,4-dihydronicotinamide [(BNA)<sub>2</sub>] with  $\text{Acr}^+-\text{Mes}$  (174%) as is the case of the  $\Phi_{\text{TET}}$  value of formation of the triplet ET state (98%).<sup>[17]</sup> The larger  $\Phi(\text{HV}^{\cdot+})$  of [(BNA)<sub>2</sub>] than those of BNAH result from the much faster C-C bond cleavage of [(BNA)<sub>2</sub>]<sup>•+</sup> to produce  $\text{BNA}^{\cdot}$  and  $\text{BNA}^+$  as compared with the deprotonation of  $\text{BNAH}^{\cdot+}$  to produce  $\text{BNA}^{\cdot}$  in competition with the back electron transfer.<sup>[31]</sup> It should be noted that the maximum  $\Phi(\text{HV}^{\cdot+})$  value should be twice of the  $\Phi_{\text{TET}}$  value, because two equivalents of  $\text{HV}^{\cdot+}$  is produced by the photoreduction of  $\text{HV}^{2+}$  by BNAH and (BNA)<sub>2</sub>.<sup>[31]</sup> As mentioned above, the  $\Phi_{\text{TET}}$  value of 98% estimated using the  $\epsilon$  value at 500 nm of  $\text{Acr}^+-1\text{NA}$  is the maximum value, because of the overlap of absorbance due to the  $\text{R}^{\cdot+}$  moiety in the triplet ET state. The maximum  $\Phi(\text{HV}^{\cdot+})$  value of 174% provides the minimum  $\Phi_{\text{TET}}$  value of 87%. Thus, the actual  $\Phi_{\text{TET}}$  value is between 87 and 98%. A parallel relationship between  $\Phi_{\text{TET}}$  and  $\Phi(\text{HV}^{\cdot+})$  in Table 4 indicates that the photocatalytic reduction of  $\text{HV}^{2+}$  was catalyzed by the long-lived triplet ET states of  $\text{Acr}^+-\text{R}$ .

**Table 4** Quantum yields of the triplet ET State ( $\Phi_{\text{TET}}$ ) of  $\text{Acr}^+-\text{R}$  and quantum yields [ $\Phi(\text{HV}^{\cdot+})$ ] of formation of  $\text{HV}^{\cdot+}$  in the photocatalytic reduction of  $\text{HV}^{2+}$  by BNAH and (BNA)<sub>2</sub>.

| Acridinium                              | $\Phi_{\text{TET}}^{\text{[a]}}$ , % | $\Phi(\text{HV}^{\cdot+})^{\text{[b]}}$ , % | $\Phi(\text{HV}^{\cdot+})^{\text{[c]}}$ , % |
|---|--------------------------------------|---|---|
| $\text{Acr}^+-\text{Tol}$               | 5                                    | 8   | 6   |
| $\text{Acr}^+-\text{Xyl}$               | 55                                   | 74  | 95  |
| $\text{Acr}^+-\text{Mes}$               | 98                                   | 100   | 174   |
| $\text{Acr}^+-\text{Dur}$               | 4                                    | 2   | 6   |
| $\text{Acr}^+-1\text{NA}$               | 36                                   | 24  | 28  |
| $\text{Acr}^+-2\text{NA}$               | 10                                   | 8   | 8   |
| $\text{Acr}^+-1\text{NA}(2\text{-Mes})$ | 23                                   | 8   | 17  |
| $\text{Acr}^+-\text{An}$                | [d]                                  | [d]   | [d]   |
| $\text{Acr}^+-2\text{NA}(6\text{-OMe})$ | [d]                                  | [d]   | [d]   |

[a] Determined from Figure 4a. [b] [BNAH] =  $2.0 \times 10^{-4}$  M; [ $\text{HV}^{2+}$ ] =  $1.0 \times 10^{-3}$  M; [ $\text{Acr}^+-\text{R}$ ] =  $2.0 \times 10^{-4}$  M. [c] [(BNA)<sub>2</sub>] =  $4.0 \times 10^{-4}$  M; [ $\text{HV}^{2+}$ ] =  $1.0 \times 10^{-3}$  M; [ $\text{Acr}^+-\text{R}$ ] =  $2.0 \times 10^{-4}$  M. [d] Too small to be determined accurately.

Since the quantum yield of formation of the triplet excited state of  $\text{Acr}^+-\text{Mes}$  is unity, exhibiting the highest photocatalytic efficiency for the one-electron reduction of  $\text{HV}^{2+}$  by BNAH (vide supra), the oxidizing and reducing abilities of the ET state ( $\text{Acr}^+-\text{Mes}^{\cdot+}$ ) are examined in detail. The triplet ET state of  $\text{Acr}^+-\text{Mes}$  is expected to act as a strong electron acceptor ( $E_{\text{red}}$  vs. SCE = 2.06 V in MeCN) as well as a strong electron donor ( $E_{\text{ox}}$  vs. SCE = -0.57 V in MeCN), which can oxidize and reduce the various substrates, respectively. We also examined the electron-transfer oxidation of various aromatic compounds by the  $\text{Mes}^{\cdot+}$  moiety. Since the one-electron reduction potential of  $\text{Acr}^+-\text{Mes}^{\cdot+}$  ( $E_{\text{red}}$  vs. SCE = 2.06 V) is more positive than that of the one-electron oxidation potential of naphthalene ( $E_{\text{ox}}$  vs. SCE = 1.80 V),<sup>[5]</sup> electron transfer from naphthalene to the  $\text{Mes}^{\cdot+}$  moiety of  $^1(\text{Acr}^+-\text{Mes}^{\cdot+})$  is energetically feasible. The rate constant of electron transfer from naphthalene to the  $\text{Mes}^{\cdot+}$  moiety of  $^1(\text{Acr}^+-\text{Mes}^{\cdot+})$  was determined from the decay of absorbance at 500 nm in the time scale of intersystem crossing to  $^3(\text{Acr}^+-\text{Mes}^{\cdot+})$  by femtosecond laser excitation to be  $1.0 \times 10^{10} \text{ M}^{-1} \text{ s}^{-1}$  as shown in Figure S8 (SI). The rate constant of electron transfer from naphthalene to the  $\text{Mes}^{\cdot+}$  moiety of  $^3(\text{Acr}^+-\text{Mes}^{\cdot+})$  was also determined by nanosecond laser excitation of a deaerated MeCN solution of  $\text{Acr}^+-\text{Mes}$  containing naphthalene at 355 nm, which resulted in the formation of naphthalene radical cation ( $\lambda_{\text{max}} = 69 \text{ nm}$ ),<sup>[38]</sup> whereas the transient absorption due to  $\text{Acr}^+-\text{Mes}$  ( $\lambda_{\text{max}} = 500 \text{ nm}$ )<sup>[17,49]</sup> remains the same as shown in Figure 6a. Transient

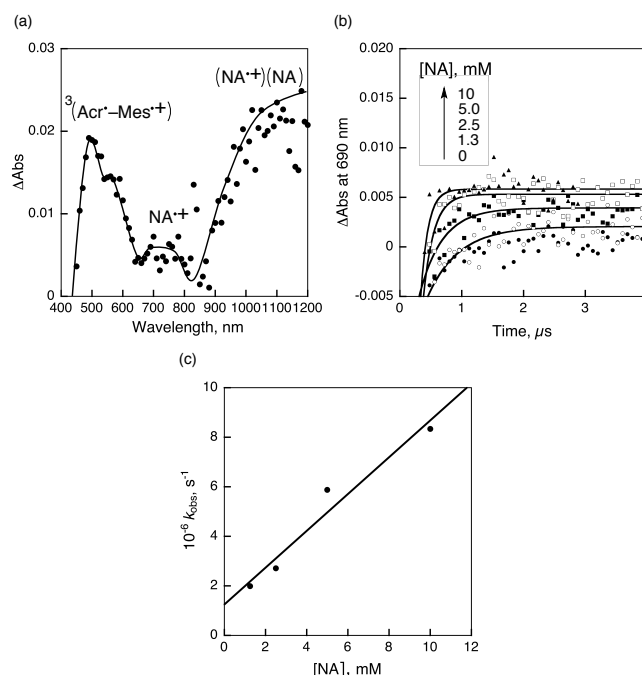


**Figure 6.** (a) Transient absorption spectra of  $\text{Acr}^+-\text{Mes}$  ( $1.0 \times 10^{-4}$  M) in the presence of NA ( $2.0 \times 10^{-1}$  M) in deaerated MeCN at 298 K taken 2  $\mu\text{s}$  after laser excitation at 355 nm. (b) Time profiles of the absorbance rise at 690 nm. (c) Rise rate constant versus concentrations of naphthalene.

absorption spectra of radical cation species of 9,10-dimethylantracene, 9-methylantracene, anthracene, fluorene, 2-methoxynaphthalene, and 1-bromonaphthalene were also observed by electron transfer from these aromatic donors to the  $\text{Mes}^{\cdot+}$  moiety of  $\text{Acr}^+-\text{Mes}^{\cdot+}$  in MeCN when the electron transfer is thermodynamically feasible (see Figure S9 in SI).<sup>[60]</sup>

Photoirradiation of an MeCN solution of  $\text{Acr}^+-\text{Mes}$  containing  $\text{HV}^{2+}$  results in formation of hexyl viologen radical cation ( $\text{HV}^{•+}$ ;  $\lambda_{\text{max}} = 605 \text{ nm}$ )<sup>[40]</sup> with a concomitant decrease in the absorption band due to the  $\text{Acr}^+$  moiety as shown in Figure 7. Electron transfer from the  $\text{Acr}^+$  moiety of  ${}^3(\text{Acr}^+-\text{Mes}^{•+})$  to  $\text{HV}^{2+}$  ( $E_{\text{red}}$  vs. SCE =  $-0.42 \text{ V}$ )<sup>[38]</sup> is energetically feasible ( $-\Delta G_{\text{ET}} = 0.15 \text{ eV}$ ). When *p*-benzoquinone (Q;  $E_{\text{red}}$  vs. SCE =  $-0.50 \text{ V}$ )<sup>[61,62]</sup> is employed instead of  $\text{HV}^{2+}$ , *p*-benzosemiquinone radical anion ( $\text{Q}^{\cdot-}$ ;  $\lambda_{\text{max}} = 400 \text{ nm}$ )<sup>[61,62]</sup> is also produced by the electron transfer from the  $\text{Acr}^+$  moiety of  ${}^3(\text{Acr}^+-\text{Mes}^{•+})$  to Q (see Figure S10 in

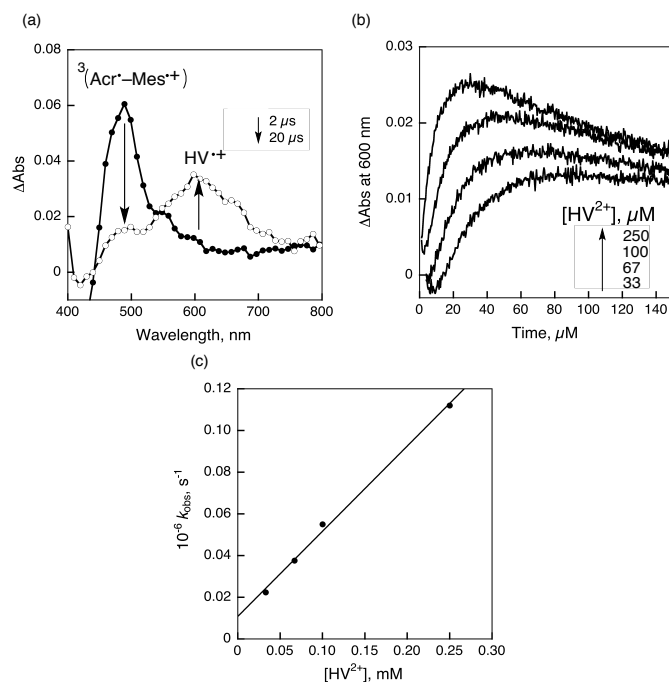


**Figure 7.** (a) Transient absorption spectra of  $\text{Acr}^+-\text{Mes}$  ( $1.0 \times 10^{-4} \text{ M}$ ) in the presence of  $\text{HV}^{2+}$  ( $5.0 \times 10^{-4} \text{ M}$ ) in deaerated MeCN at 298 K taken 2  $\mu\text{s}$  (●) and 20  $\mu\text{s}$  (○) after laser excitation at 355 nm. (b) Time profiles of the absorbance rise at 600 nm. (c) Rise rate constant versus concentrations of  $\text{HV}^{2+}$ .

**Table 5** One-electron oxidation of electron donors and reduction potentials of electron acceptors and rate constants of electron transfer from electron donors to the triplet ET state of  $\text{Acr}^+-\text{Mes}$  and from the triplet ET state of  $\text{Acr}^+-\text{Mes}$  to electron acceptors.

| electron donor                         | $E_{\text{ox}}$ vs. SCE, V  | $-\Delta G_{\text{et}}$ , eV | $k_{\text{et}}$ , $\text{M}^{-1} \text{s}^{-1}$ |
|--|-----------------------------|------------------------------|---|
| 1-bromonaphthalene                     | 1.94                        | 0.12                         | $1.9 \times 10^5$                               |
| naphthalene                            | 1.80                        | 0.26                         | $7.4 \times 10^8$                               |
| 2-methoxynaphthalene <sup>[a]</sup>    | 1.52                        | 0.54                         | $1.9 \times 10^9$                               |
| fluorene <sup>[a]</sup>                | 1.45                        | 0.61                         | $4.1 \times 10^9$                               |
| anthracene <sup>[a]</sup>              | 1.19                        | 0.87                         | $7.5 \times 10^9$                               |
| 9-methylanthracene <sup>[a]</sup>      | 1.11                        | 0.95                         | $1.3 \times 10^{10}$                            |
| 9,10-dimethylanthracene <sup>[a]</sup> | 1.05                        | 1.01                         | $1.4 \times 10^{10}$                            |
| electron acceptor                      | $E_{\text{red}}$ vs. SCE, V | $-\Delta G_{\text{et}}$ , eV | $k_{\text{et}}$ , $\text{M}^{-1} \text{s}^{-1}$ |
| <i>p</i> -benzoquinone                 | $-0.55$                     | 0.07                         | $3.0 \times 10^7$                               |
| $\text{HV}^{2+}$                       | $-0.42$                     | 0.15                         | $4.1 \times 10^8$                               |
| TCNQ                                   | 0.17                        | 0.74                         | $2.7 \times 10^9$                               |

[a] Taken from ref. [60a].

SI). We also examined the electron-transfer reduction of TCNQ by the  $\text{Acr}^+$  moiety of  ${}^3(\text{Acr}^+-\text{Mes}^{•+})$  (Figure S11 in SI). The rate constants of the electron-transfer reduction of electron acceptors by the  $\text{Acr}^+$  moiety of  ${}^3(\text{Acr}^+-\text{Mes}^{•+})$  are listed in Table 5 together with the driving force of electron transfer. As shown in Table 5,  ${}^3(\text{Acr}^+-\text{Mes}^{•+})$  acts as both an electron donor and acceptor.<sup>[63]</sup> The driving force dependence of the rate constants of electron-transfer reactions of  ${}^3(\text{Acr}^+-\text{Mes}^{•+})$  with electron donors and acceptors is shown in Figure 8. The solid line is drawn by using the Marcus equation for intermolecular outer-sphere electron transfer reactions [Equation (3)],

$$1/k_{\text{et}} = 1/k_{\text{diff}} + 1/[Z \exp\{-\lambda/4(1 + \Delta G_{\text{et}}/\lambda)^2/k_{\text{B}}T\}] \quad (3)$$

where  $Z$  is the collision frequency taken as  $1 \times 10^{11} \text{ M}^{-1} \text{ s}^{-1}$ ,  $\lambda$  is the reorganization energy of electron transfer,  $k_{\text{B}}$  is the Boltzmann constant, and  $T$  is the absolute temperature.<sup>[15,64]</sup> The  $\lambda$  value is determined to be 1.0 eV as the best fit value of Equation (3) and this value is larger than the value obtained for intramolecular photoinduced ET and BET of  $\text{Acr}^+-\text{R}$  (Figure 5), because a large solvent reorganization is required for intermolecular ET compared with intramolecular ET. The driving force dependence of  $\log k_{\text{et}}$  for intermolecular electron transfer from electron donor to the  $\text{Mes}^{•+}$  moiety and also from the  $\text{Acr}^+$  moiety in the triplet E' state [ ${}^3(\text{Acr}^+-\text{Mes}^{•+})$ ] to electron acceptors in MeCN clearly indicates that the photogenerated species is the triplet ET state which is capable of not only oxidizing electron donors but also reducing electron acceptors as long as the one-electron oxidation potentials of electron donors are lower (less positive) than the one-electron oxidation potential of  $\text{Acr}^+-\text{Mes}$  and the one-electron reduction potentials of electron acceptors are higher (more positive) than the one-electron reduction potential of  $\text{Acr}^+-\text{Me}$  (note that the redox potentials are somewhat different depending on the solvent in Table 2). The locally excited triplet state of  $\text{Acr}^+-\text{Mes}$  would never be able to oxidize electron donors with the oxidation potentials higher than 1.53 V (vs. SCE) and to reduce electron acceptors lower than 0.07 V (vs. SCE) as discussed in Introduction.

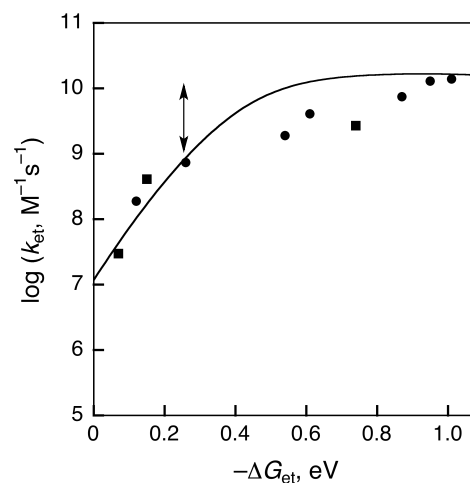


**Figure 8.** Driving force dependences of  $\log k_{\text{et}}$  for electron transfer from electron donors (●) to  $\text{Mes}^{•+}$  and from  $\text{Acr}^+$  in the triplet ET state of  $\text{Acr}^+-\text{Mes}^{•+}$  to electron acceptors (■) in MeCN at 298 K and the fit of the curve based on the Marcus theory of electron transfer [Equation (3)].

The  $k_{\text{et}}$  value of electron transfer from naphthalene to  $^1(\text{Acr}^+ - \text{Mes}^{++})$  ( $1.0 \times 10^{10} \text{ M}^{-1} \text{ s}^{-1}$ ) is ten times larger than that of electron

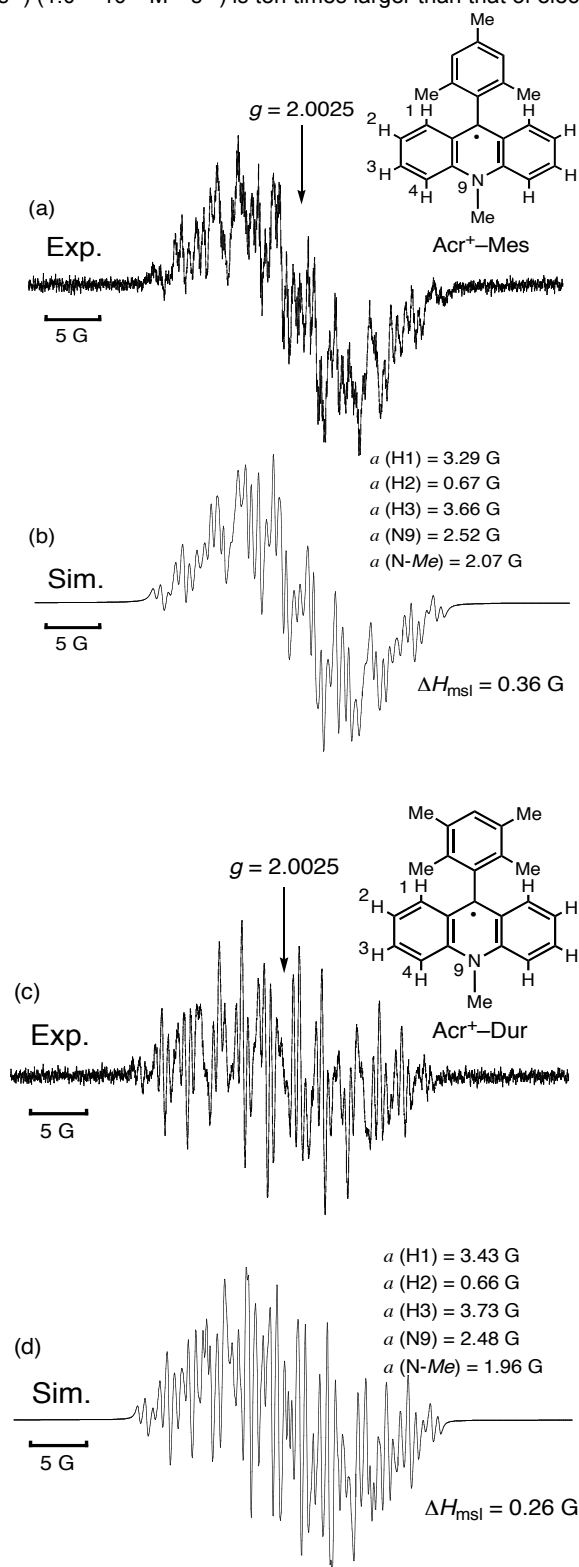


**Figure 9.** (a) ESR spectrum of  $\text{Acr}^+ - \text{Mes}$  in deaerated MeCN at 298 K and (b) the computer simulated spectrum with the  $hfc$  and  $\Delta H_{\text{msl}}$  values. (c) ESR spectrum of  $\text{Acr}^+ - \text{Dur}$  in deaerated MeCN at 298 K and (d) the computer simulated spectrum with the  $hfc$  and  $\Delta H_{\text{msl}}$  values.

transfer from the same naphthalene to  $^3(\text{Acr}^+ - \text{Mes}^{++})$  ( $7.4 \times 10^8 \text{ M}^{-1} \text{ s}^{-1}$ ). Such a difference in the  $k_{\text{et}}$  value results from the higher energy of the singlet ET state as compared with the triplet ET state. The singlet-triplet energy gap may be smaller than 0.1 eV because the singlet excited state of the  $\text{Acr}^+$  moiety of  $\text{Acr}^+ - \text{Mes}$  (2.73 eV) is only by 0.1 eV higher than the energy of the triplet ET state (2.63 eV in PhCN). If the energy of the singlet ET state is higher than 2.73 eV, electron transfer from the Mes moiety to the singlet excited state of the  $\text{Acr}^+$  moiety would be endergonic.

**Origin of the large difference in the ET quantum yields of  $\text{Acr}^+ - \text{R}$ .** Large quantum yields ( $\Phi_{\text{ET}}$ ) of formation of the long-lived triplet ET states of  $\text{Acr}^+ - \text{R}$  in Table 4 are obtained when the orientation of the R and  $\text{Acr}^+$  moieties is nearly orthogonal (see Table 1). Thus, introduction of a substituent at the ortho-position seems essential to minimize the interaction between the R and  $\text{Acr}^+$  moieties and to attain large quantum yields of the long-lived ET states. However, the triplet ET quantum yield of  $\text{Acr}^+ - \text{Du}$  (4%) is significantly lower than that of  $\text{Acr}^+ - \text{Mes}$  (98%), although both dihedral angles are nearly  $90^\circ$ . The  $E_{\text{ox}}$  values of the Me and Dur moieties are also virtually the same. In order to examine the difference in the orbital interaction between R = Mes and Dur the one-electron reduced radicals,  $\text{Acr}^+ - \text{Mes}$  and  $\text{Acr}^+ - \text{Dur}$ , were produced by the one-electron reduction of  $\text{Acr}^+ - \text{Mes}$  and  $\text{Acr}^+ - \text{Dur}$  by tetramethylsemiquinone radical anion and the ESR spectra are measured as shown in Figure 9.<sup>[16]</sup> The hyperfine splitting constants ( $hfc$ ) and the maximum slope line width ( $\Delta H_{\text{msl}}$ ) were determined by computer simulation of the ESR spectra. The  $hfc$  values thus determined are given in Figure 9. The assignment of the  $hfc$  values was made based on comparison of the observed  $hfc$  values with those predicted by DFT calculation (see Experimental Section). There is no appreciable difference in the  $hfc$  values between  $\text{Acr}^+ - \text{Mes}$  and  $\text{Acr}^+ - \text{Dur}$  and no spin is delocalized on the donor moieties as expected by the orthogonal orientation between the donor and acceptor moieties. This shows sharp contrast with the case of  $\text{Acr}^+ - \text{Ph}$  in which the unpaired spin is delocalized on the Ph moiety,<sup>[16]</sup> as expected from the non-orthogonal orientation between the Ph and  $\text{Acr}^+$  moieties (the dihedral angle is  $68^\circ$ ).<sup>[43,44]</sup>

In contrast with the case of the one-electron reduced species of  $\text{Acr}^+ - \text{Mes}$  and  $\text{Acr}^+ - \text{Dur}$ , which exhibited no appreciable difference in the  $hfc$  values, the calculated  $hfc$  values of hydrogen atoms of 2- and 6-methyl groups of the one-electron oxidized

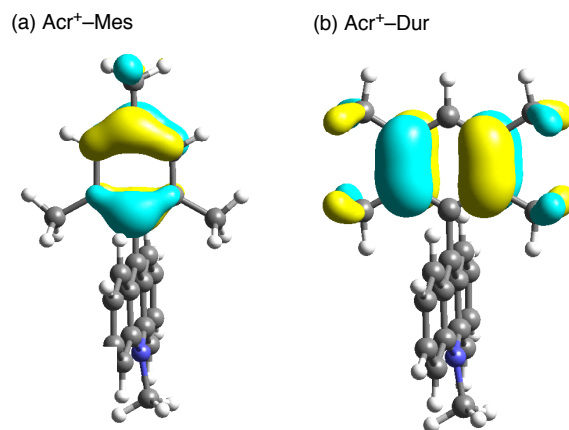


**Figure 10.** HOMO orbitals of (a)  $\text{Acr}^+ - \text{Mes}$  and (b)  $\text{Acr}^+ - \text{Dur}$  calculated by a DFT method at B3LYP/6-31G(d) level.

species are quite different between  $\text{Acr}^+-\text{Mes}^{++}$  and  $\text{Acr}^+-\text{Dur}^{++}$ : the  $hfc$  value of  $\text{Acr}^+-\text{Dur}^{++}$  is 11.8 G, whereas those of  $\text{Acr}^+-\text{Mes}^{++}$  is 0 G.<sup>[65]</sup> Such a drastic difference results from the disappearance in the unpaired spin at the *ortho*-position in  $\text{Acr}^+-\text{Mes}$  (see the spin distributions in Figure 10). The large spin distribution on 2- and 6-methyl groups of the orbital interaction between the  $\text{Dur}^{++}$  and  $\text{Acr}^+$  moieties of  $\text{Acr}^+-\text{Dur}^{++}$  is expected to the durene moiety of  $\text{Acr}^+-\text{Dur}^{++}$  results from the  $\sigma^*-\pi^*$  hyperconjugation. In such a case, the interaction between the  $\text{Dur}^{++}$  and  $\text{Acr}^+$  moieties of  $\text{Acr}^+-\text{Dur}^{++}$  would be much larger than that between the  $\text{Mes}^{++}$  and  $\text{Acr}^+$  moieties of  $\text{Acr}^+-\text{Mes}^{++}$ , despite the orthogonal orientation between the donor and acceptor moieties in both cases, resulting in the fast back electron transfer in the singlet ET state in competition with the intersystem crossing to afford the long lived triplet ET state.

## Conclusion

In conclusion, we have obtained a bell-shaped driving force dependence of rates of intramolecular photoinduced ET including the BET rate constants in 9-substituted 10-methylacridinium ions ( $\text{Acr}^+-\text{R}$ ). The ET states of  $\text{Acr}^+-\text{R}$  are extremely long-lived except for  $\text{R} = \text{An}$  because of the small reorganization energy of electron transfer and the high energy of the triplet ET states which are lower than the locally excited triplet states. In particular, the quantum yield of the extremely long-lived ET state of  $\text{Acr}^+-\text{Mes}$  is the highest among  $\text{Acr}^+-\text{R}$ , being close to unity, because of weak orbital interaction between the donor and acceptor moiety in the ET state. This makes  $\text{Acr}^+-\text{Mes}$  the most efficient organic photocatalyst available for construction of energy conversion systems and synthetic applications.

## Acknowledgments

This work was supported by Grants-in-Aid (no. 16H02268 to S.F., 16K13964, 26620154 and 26288037 to K.O.) from the Ministry of Education, Culture, Sports, Science and Technology (MEXT); SENTAN projects from JST, Japan (to S.F.).

**Keywords:** photoredox catalyst • charge separation • transient absorption spectroscopy • donor-acceptor system

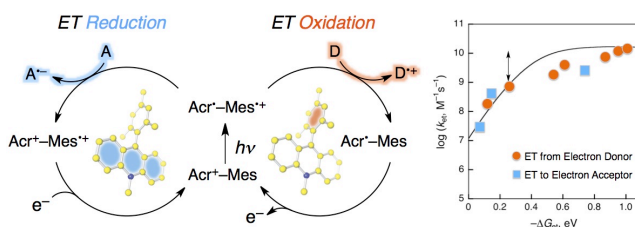
- [1] *The Photosynthetic Reaction Center*, J. Deisenhofer, J. R. Norris, Eds., Academic Press, San Diego, **1993**.
- [2] a) *Anoxygenic Photosynthetic Bacteria* (Eds.: R. E. Blankenship, M. T. Madigan, C. E. Bauer), Kluwer Academic Publisher, Dordrecht, **1995**; b) *Molecular Level Artificial Photosynthetic Materials*, G. J. Meyer, Wiley, New York, **1997**.
- [3] a) R. A. Wheeler, *Introduction to the Molecular Bioenergetics of Electron, Proton, and Energy Transfer*: ACS Symposium Series **2004**, 883, 1; b) W. Leibl, P. Mathis, *Electron Transfer in Photosynthesis. Series on Photoconversion of Solar Energy*, **2004**, 2, 117.
- [4] a) B. D. Sherman, M. D. Vaughn, J. J. Bergkamp, D. Gust, A. L. Moore, T. A. Moore, *Photosynth. Res.* **2014**, 120, 5; b) D. Gust, T. A. Moore, A. L. Moore, *Acc. Chem. Res.* **2009**, 42, 1890.
- [5] a) M. Rudolf, S. V. Kirner, D. M. Guldi, *Chem. Soc. Rev.* **2016**, 45, 612; b) G. Bottari, G. de la Torre, D. M. Guldi, T. Torres, *Chem. Rev.* **2010**, 110, 6768; c) V. Sgobba, D. M. Guldi, *Chem. Soc. Rev.* **2009**, 38, 165.
- [6] M. R. Wasielewski, *Acc. Chem. Res.* **2009**, 42, 1910.
- [7] S. Fukuzumi, *Phys. Chem. Chem. Phys.* **2008**, 10, 2283.
- [8] a) F. D'Souza, O. Ito, *Chem. Commun.* **2009**, 4913; b) F. D'Souza, O. Ito, *Coord. Chem. Rev.* **2005**, 249, 1410; c) M. E. El-Khouly, S. Fukuzumi, F. D'Souza, *ChemPhysChem* **2014**, 15, 30.
- [9] S. Fukuzumi, K. Saito, K. Ohkubo, T. Khoury, Y. Kashiwagi, M. A. Absalom, S. Gadde, F. D'Souza, Y. Araki, O. Ito, M. Crossley, *Chem. Commun.* **2011**, 47, 7980.
- [10] a) T. Kojima, T. Honda, K. Ohkubo, M. Shiro, T. Kusukawa, T. Fukuda, N. Kobayashi, S. Fukuzumi, *S. Angew. Chem., Int. Ed.* **2008**, 47, 6712; b) S. Fukuzumi, T. Honda, K. Ohkubo, T. Kojima, *Dalton Trans.* **2009**, 3880; c) T. Kojima, K. Hanabusa, K. Ohkubo, M. Shiro, S. Fukuzumi, *Chem.-Eur. J.* **2010**, 16, 3646.
- [11] S. Fukuzumi, *In Functional Organic Materials* (Eds.: T. J. J. Müller, U. H. F. Bunz), Wiley-VCH, **2007**, 465.
- [12] H. Imahori, Y. Sekiguchi, Y. Kashiwagi, T. Sato, Y. Araki, O. Ito, H. Yamada, S. Fukuzumi, *Chem.-Eur. J.* **2004**, 10, 3184.
- [13] J.-R. Shen, *Annu. Rev. Plant Biol.* **2015**, 66, 23.
- [14] A. Harriman, *Angew. Chem., Int. Ed.* **2004**, 43, 4985.
- [15] a) R. A. Marcus, *Angew. Chem., Int. Ed. Engl.* **1993**, 32, 1111; b) R. A. Marcus, N. Sutin, *Biochim. Biophys. Acta* **1985**, 811, 265.
- [16] S. Fukuzumi, K. Ohkubo, T. Suenobu, K. Kato, M. Fujitsuka, O. Ito, *J. Am. Chem. Soc.* **2001**, 123, 8459.
- [17] S. Fukuzumi, H. Kotani, K. Ohkubo, S. Ogo, N. V. Tkachenko, I. Lemmetyinen, *J. Am. Chem. Soc.* **2004**, 126, 1600.
- [18] a) A. C. Benniston, K. J. Elliott, R. W. Harrington, W. Clegg, *Eur. J. Org. Chem.* **2009**, 253; b) A. C. Benniston, A. Harriman, P. Li, J. P. Rostron, I. J. van Ramesdonk, M. M. Groeneveld, H. Zhang, J. W. Verhoeven, *J. Am. Chem. Soc.* **2005**, 127, 16054; c) A. C. Benniston, A. Harriman, P. Li, J. F. Rostron, J. W. Verhoeven, *Chem. Commun.* **2005**, 2701; d) A. C. Benniston, A. Harriman, J. W. Verhoeven, *Phys. Chem. Chem. Phys.* **2008**, 10, 5156.
- [19] K. Ohkubo, H. Kotani, S. Fukuzumi, *Chem. Commun.* **2005**, 4520.
- [20] a) S. Fukuzumi, K. Ohkubo, T. Suenobu, *Acc. Chem. Res.* **2014**, 47, 1455; b) S. Fukuzumi, K. Ohkubo, *Chem. Sci.* **2013**, 4, 561.
- [21] a) N. A. Romero, D. A. Nicewicz, *Chem. Rev.* **2016**, 116, 10075; b) K. I. Margrey, D. A. Nicewicz, *Acc. Chem. Res.* **2016**, 49, 1997.
- [22] a) N. A. Romero, K. A. Margrey, N. E. Tay, D. A. Nicewicz, *Science* **2011**, 349, 1326; b) C. L. Cavanaugh, D. A. Nicewicz, *Org. Lett.* **2015**, 17, 6082.
- [23] a) N. A. Romero, D. A. Nicewicz, *J. Am. Chem. Soc.* **2014**, 136, 17024; b) D. J. Wilger, J. M. Grandjean, T. Lammert, D. A. Nicewicz, *Nat. Chem.* **2014**, 6, 720; c) T. M. Nguyen, N. Manohar, D. A. Nicewicz, *Angew. Chem., Int. Ed.* **2014**, 53, 6198; d) D. A. Nicewicz, D. S. Hamilton, *Synle* **2014**, 25, 1191; e) A. J. Perkowski, D. A. Nicewicz, *J. Am. Chem. Soc.* **2013**, 135, 10334; f) T. M. Nguyen, D. A. Nicewicz, *J. Am. Chem. Soc.* **2013**, 135, 9588; g) D. J. Wilger, N. J. Gesmundo, D. A. Nicewicz, *Chem. Sci.* **2013**, 4, 3160; h) D. S. Hamilton, D. A. Nicewicz, *J. Am. Chem. Soc.* **2012**, 134, 18577; i) D. A. Nicewicz, T. M. Nguyen, *ACS Catal.* **2014**, 4, 355.
- [24] S. Fukuzumi, A. Ito, T. Suenobu, K. Ohkubo, *J. Phys. Chem. C* **2014**, 118, 24188.
- [25] a) N. Xu, P. Li, Z. Xie, L. Wang, *Chem.-Eur. J.* **2016**, 22, 2236; b) A. J. Perkowski, C. L. Cruz, D. A. Nicewicz, *J. Am. Chem. Soc.* **2015**, 137, 15684; c) P. D. Morse, D. A. Nicewicz, *Chem. Sci.* **2015**, 6, 270; d) Y. Gu, K. Ellis-Guardiola, P. Srivastava, J. C. Lewis, *ChemBioChem* **2015**, 16, 1880.
- [26] a) C. Cassani, G. Bergonzini, C.-J. Wallentin, *Org. Lett.* **2014**, 16, 4228; b) T. Chinzai, K. Miyazawa, Y. Yasu, T. Koike, M. Akita, *RSC Adv.* **2015**, 5, 21297; c) M. A. Zeller, M. Riener, D. A. Nicewicz, *Org. Lett.* **2014**, 16, 4810; d) J. Grandjean, D. A. Nicewicz, *Angew. Chem., Int. Ed.* **2013**, 52, 3967.
- [27] T. Hering, A. U. Mayer, B. König, *J. Org. Chem.* **2016**, 81, 6927.
- [28] T. Nakagawa, K. Okamoto, H. Hanada, R. Katoh, *Opt. Lett.* **2016**, 41, 1498.
- [29] W. L. F. Armarego, C. L. L. Chai, *Purification of Laboratory Chemicals*, 6th ed., Butterworth-Heinemann, Amsterdam, **2009**.
- [30] S. Fukuzumi, S. Koumitsu, K. Hironaka, T. Tanaka, *J. Am. Chem. Soc.* **1987**, 109, 305.
- [31] a) S. Fukuzumi, T. Suenobu, M. Patz, T. Hirasaka, S. Itoh, M. Fujitsuka, O. Ito, *J. Am. Chem. Soc.* **1998**, 120, 8060; b) M. Patz, Y. Kuwahara, T. Suenobu, S. Fukuzumi, *Chem. Lett.* **1997**, 567.
- [32] S. Fukuzumi, H. Imahori, H. Yamada, M. E. El-Khouly, M. Fujitsuka, O. Ito,

- D. M. Guldi, *J. Am. Chem. Soc.* **2001**, *123*, 2571.
- [33] J. Bruinink, C. G. A. Kregting, J. J. Ponjee, *J. Electrochem. Soc.* **1977**, *124*, 1854.
- [34] H. Kotani, K. Ohkubo, S. Fukuzumi, *J. Am. Chem. Soc.* **2004**, *126*, 15999.
- [35] The SHACV method provides a superior approach to directly evaluating the one-electron redox potentials in the presence of a follow-up chemical and reaction, relative to the better-known dc and fundamental harmonic ac methods. See: a) M. R. Wasielewski, R. Breslow, *J. Am. Chem. Soc.* **1976**, *98*, 4222; b) E. M. Arnett, K. Amarnath, N. G. Harvey, J. Cheng, *J. Am. Chem. Soc.* **1990**, *112*, 344.
- [36] C. K. Mann, K. K. Barnes, *Electrochemical Reactions in Non-aqueous Systems*, Mercel Dekker, New York, **1970**.
- [37] Femtosecond fluorescence decays and time-resolved transient absorption spectra were measured by an up-conversion and pump-probe methods as described previously. See: N. V. Tkachenko, L. Rantala, A. Y. Tauber, J. Helaja, P. H. Hynninen, H. Lemmetyinen, *J. Am. Chem. Soc.* **1999**, *121*, 9378.
- [38] C. Luo, M. Fujitsuka, A. Watanabe, O. Ito, L. Gan, Y. Huang, C.-H. Haung, *J. Chem. Soc., Faraday Trans.* **1998**, *94*, 527.
- [39] G. J. Kavarnos, *Fundamental of Photoinduced Electron Transfer*, Wiley-VCH, New York, **1993**.
- [40] S. Fukuzumi, H. Imahori, K. Okamoto, H. Yamada, M. Fujitsuka, O. Ito, D. M. Guldi, *J. Phys. Chem. A* **2002**, *106*, 1903.
- [41] a) A. D. Becke, *J. Chem. Phys.* **1993**, *98*, 5648; b) C. Lee, W. Yang, R. G. Parr, *Phys. Rev. B* **1988**, *37*, 785; c) W. J. Hehre, L. Radom, P. v. R. Schleyer, J. A. Pople, *Ab Initio Molecular Orbital Theory*, Wiley, New York, **1986**.
- [42] The exciplex emission was observed for R = 1NA and 2NA at 594 nm and 590 nm, respectively.
- [43] K. Goubitz, C. A. Reiss, D. Heijdenrijk, S. A. Jonker, J. W. Verhoeven, *Acta Cryst.* **1989**, *C45*, 1348.
- [44] C. A. Reiss, K. Goubitz, D. Heijdenrijk, *Acta Cryst.* **1989**, *C45*, 1350.
- [45] S. Fukuzumi, K. Ohkubo, Y. Tokuda, T. Suenobu, *J. Am. Chem. Soc.* **2000**, *122*, 4286.
- [46] K. Ohkubo, K. Suga, K. Morikawa, S. Fukuzumi, *J. Am. Chem. Soc.* **2003**, *125*, 12850.
- [47] M. Tanaka, K. Yukimoto, K. Ohkubo, S. Fukuzumi, *J. Photochem. Photobiol. A* **2008**, *197*, 206.
- [48] a) T. Shida, S. Iwata, *J. Am. Chem. Soc.* **1973**, *95*, 3473; b) F. Cataldo, S. Iglesias-Groth, A. Manchado, *Spectrochim. Acta A* **2010**, *77*, 998.
- [49] S. Fukuzumi, H. Kotani, K. Ohkubo, *Phys. Chem. Chem. Phys.* **2008**, *10*, 5159.
- [50] S. F. Nelsen, M. N. Weaver, D. Yamazaki, K. Komatsu, R. Rathore, T. Bally, *J. Phys. Chem. A* **2007**, *111*, 1667.
- [51] H. Friha, G. Féraud, T. Troy, C. Falvo, P. Parneix, P. Bréchnignac, Z. Dhaouadi, T. W. Schmidt, T. Pino, *J. Phys. Chem. A* **2013**, *117*, 13664.
- [52] K. Hall, M. Boggio-Pasqua, M. Bearpark, M. Robb, *J. Phys. Chem. A* **2006**, *110*, 13591.
- [53] K. R. Naqvi, T. B. Melø, *Chem. Phys. Lett.* **2006**, *428*, 83.
- [54] R. S. H. Liu, R. E. Kellogg, *J. Am. Chem. Soc.* **1969**, *91*, 250.
- [55] S. Fukuzumi, K. Doi, A. Itoh, T. Suenobu, K. Ohkubo, Y. Yamada, K. D. Karlin, *Proc. Natl. Acad. Sci. U.S.A.* **2012**, *109*, 15572.
- [56] Larger *V* values have been reported for photoinduced ET in electron donor-acceptor dyads. See: a) M. Bixon, J. Jortner, J. W. Verhoeven, *J. Am. Chem. Soc.* **1994**, *116*, 7349; b) R. M. Williams, M. Koeberg, J. M. Lawson, Y.-Z. An, Y. Rubin, M. N. Paddon-Row, J. W. Verhoeven, *J. Org. Chem.* **1996**, *61*, 5055; c) S. V. Rosokha, D.-L. Sun, J. K. Kochi, *J. Phys. Chem. A* **2002**, *106*, 2283; d) H. Imahori, N. V. Tkachenko, V. Vehmanen, K. Tamaki, H. Lemmetyinen, Y. Sakata, S. Fukuzumi, *J. Phys. Chem. A* **2001**, *105*, 1750. The relatively small *V* value in the present case results from little interaction between the R and Acr<sup>+</sup> moieties in Acr<sup>+</sup>-R as described in the section of spectral and redox properties of Acr<sup>+</sup>-R.
- [57] I. R. Gould, S. Farid, *Acc. Chem. Res.* **1996**, *29*, 522.
- [58] Thermal hydride transfer from BNAH to Acr<sup>+</sup>-R is negligible because determination of  $\Phi(\text{HV}^{2+})$  was carried out under low concentrations of BNAH and HV<sup>2+</sup> (see Experimental Section). Slow thermal hydride transfer has been reported; see a) J. Hajdu, D. S. Sigman, *J. Am. Chem. Soc.* **1975**, *97*, 3524; b) J. W. Bunting, V. S. F. Chew, G. Chu, N. P. Fitzgerald, A. Gunasekara, H. T. P. Oh, *Bioorg. Chem.* **1984**, *12*, 141.
- [59] a) K. Brüggermann, R. S. Czernuszewicz, J. K. Kochi, *J. Phys. Chem.* **1992**, *96*, 4405; b) I. R. Gould, D. Ege, J. E. Moser, S. Farid, *J. Am. Chem. Soc.* **1990**, *112*, 4290.
- [60] a) H. Kotani, K. Ohkubo, S. Fukuzumi, *Appl. Catal. B: Environ.* **2008**, *7*, 317; b) K. Ohkubo, K. Mizushima, R. Iwata, S. Fukuzumi, *Chem. Sci.* **2011**, *2*, 715.
- [61] S. Fukuzumi, T. Okamoto, K. Ohkubo, *J. Phys. Chem. A* **2003**, *107*, 5412.
- [62] S. Fukuzumi, K. Ohkubo, T. Okamoto, *J. Am. Chem. Soc.* **2002**, *124*, 14147.
- [63] The triplet excited state of the Acr<sup>+</sup> moiety is certainly not involved in the photoexcitation of Acr<sup>+</sup>-Mes, because the triplet excited state of the Acr<sup>+</sup> moiety has no reducing ability.
- [64] Equation (3) has been applied to many intermolecular electron-transfer reactions; see: a) A. Apostolopoulou, M. Vlasios, P. A. Tziouris, C. Tsiafoulis, A. C. Tsipis, D. Rehder, T. A. Kabanos, A. D. Karamidas, E. Stathatos, *Inorg. Chem.* **2015**, *54*, 3979; b) Y.-M. Lee, H. Kotani, T. Suenobu, W. Nam, S. Fukuzumi, *J. Am. Chem. Soc.* **2008**, *130*, 434; c) Y. Morimoto, Y.-M. Lee, W. Nam, S. Fukuzumi, *J. Am. Chem. Soc.* **2011**, *133*, 5236; d) P. Comba, S. Fukuzumi, H. Kotani, S. Wunderlich, *Angew. Chem., Int. Ed.* **2010**, *49*, 2622; e) J. Park, Y. Morimoto, Y.-M. Lee, Y. You, W. Nam, S. Fukuzumi, *Inorg. Chem.* **2011**, *50*, 11612; f) T. Takahashi, T. Kurahashi, H. Fujii, *Inorg. Chem.* **2011**, *50*, 6922; g) K. Ohkubo, S. Fukuzumi, *J. Phys. Chem. A* **2005**, *109*, 1105; h) M. Murakan, K. Ohkubo, S. Fukuzumi, *Chem.-Eur. J.* **2010**, *16*, 7820.
- [65] The DFT calculations of Acr<sup>+</sup>-R<sup>+</sup> were performed using the B3LYP/6-31G(d) basis set.

Received: ((will be filled in by the editorial staff  
 Revised: ((will be filled in by the editorial staff  
 Published online: ((will be filled in by the editorial staff

**Entry for the Table of Contents (Please choose one layout only)**

The photoexcitation of 9-mesityl-10-methylacridinium ion ( $\text{Acr}^+-\text{Mes}$ ) results in formation of the triplet electron-transfer state, which has a long lifetime, a high energy (2.37 eV) and a high quantum yield (>75%) in acetonitrile, providing both the oxidizing and reducing activity of the  $\text{Mes}^{++}$  and  $\text{Acr}^+$  moieties, respectively.



Takeshi Tsudaka,  
Hiroaki Kotani, Kei  
Ohkubo,\* Tatsuo  
Nakagawa, Nikolai V.  
Tkachenko,\* Helge  
Lemmetyinen,\* and  
Shunichi Fukuzumi\*

Page No. – Page No.

**Photoinduced  
Electron Transfer in  
9-Substituted 10-  
Methylacridinium  
Ions**